universität wien

DIPLOMARBEIT

Titel der Diplomarbeit

“Hedgehog signalling – studies on its impact on mitochondrial function in 3T3-L1 adipocytes“

Verfasser

Lukas Frank

angestrebter akademischer Grad

Magister der Naturwissenschaften (Mag.rer.nat.)

Wien, 2012

Studienkennzahl lt. Studienblatt:	A490
Studienrichtung lt. Studienblatt:	Diplomstudium Molekulare Biologie
Betreuerin / Betreuer:	ao. Univ.-Prof. Mag. Dr. Johann Rotheneder

ACKNOWLEDGEMENTS

First of all I would like to thank my supervisor Harald Esterbauer who gave me the opportunity to work on such a wonderful and challenging project. I am very grateful for his support and guidance during my diploma studies.

Next I would like to thank Johannes Rotheneder for his great work as co-supervisor at the University of Vienna.

My thanks also to Karin Nowikovsky, Goran Mitulovic, Marion Gröger and Lukas Kenner for their excellent support throughout the whole project and their constructive criticism and advice.

I am thankful to all my colleagues, especially to Martina Bayer and Sabine Amann for their constant encouragement, ideas, support and motivation.

Finally, I would like to express my deepest appreciation to my parents Michaela and Wolfgang and to my sister Melanie, who have always encouraged me to follow my career goals and interests. Thank you for your enormous support.

TABLE OF CONTENTS

TABLE OF FIGURES

TABLE OF TABLES

LIST OF ABBREVIATIONS

1D-GeLC/MSMS	1D-gel liquid chromotography/tandem mass spectrometry
1D-PAGE	1D-polyacrylamide gel electrophoresis
AA	Acryl amide
ACN	Acetonitrile
ADP	Adenosine diphosphate
AMPK	AMP-activated protein kinase
APS	Ammonium persulfate
ATCC	American type culture collection
ATP	Adenosine triphosphate
BAT	Brown adipose tissue
BMI	Body mass index
BOC	Brother of CDO
Boi	Brother of iHog
BPB	Bromphenolblue
BSA	Bovine serum albumin
c-myc	myelocytomatosis oncogene
CAC	Citric acid cycle
CCCP	Carbonyl cyanide m-chloro phenyl hydrazone
CCL2	Chemokine (C-C motif) ligand 2
cDNA	Complementary DNA
CDO	Cell-adhesion molecule-related, down-regulated by oncogenes
CHAPS	3-[(3-cholamidopropyl)dimethylammonio]-1-propanesulfonate
Ci	Cubitus interruptus
Ci^A	Ci in a transcriptional active form
Ci^R	Ci in a transcriptional repressive form
CM	Crude mitochondria
Cos2	Costal2
COX	Cyclooxygenase
CREB	cAMP response element-binding
CS	Calf Serum
Dctn2	Dynactin subunit 2
ddH_2O	Water double distilled
DEX	Dexamethasone
DHH	Desert hedgehog
DISP	Dispatched
DMEM	Dulbecco's modified eagle's medium
DNA	Deoxyribonucleic acid
Dnm1	yeast orthologue of Drp1
Drp1	dynamin-related protein1
dsDNA	Double stranded DNA
DTT	1,4-Dithio-D,L threitol
EDTA	Ethylenediaminetetraacetic acid
ER	Endoplasmatic reticulum
ERR	Estrogen-related receptors
ES	Enrichment score
ESI	Electrospray ionization
ETC	Electron transport chain
FA	Formic Acid

FACS	Fluorescence-activated cell sorting
$FADH_2$	Reduced form of flavin adenine dinucleotide
FBS	Fetal Bovine Serum
FCCP	Carbonyl cyanide-p-trifluoromethoxyphenylhydrazone
FDR	False discovery rate
FFA	Free fatty acids
Fis1	Fission1
FSC	Forward scatter
Fzo1	Yeast orthologue of Mitofusin
GA	Glutaraldehyde
GABP	GA-binding protein
GANT	Gli Antagonist
GLI	Glioma-associated
GO	Gene ontology
GSEA	Gene set enrichment analysis
HAc	Acetic acid
HEPES	4-(2-hydroxyethyl)-1-piperazineethanesulfonic acid
Hh	Hedgehog
HhN	N-terminal Hh signalling domain
HI	Heat inactivated
HRP	Horse radish peroxidise
IAA	Iodoacetamide
IHH	Indian hedgehog
iHog	Interference hedgehog
IL-1β	Interleukin-1β
IMBX	3-isobutyl-1-methylxanthine
IMS	Intermembrane space
Kif	Kinesin family
MALDI	Matrix-assisted laser desorption/ionization
Mfn1	Mitofusin1
Mfn2	Mitofusin2
Mgm1	Yeast orthologue of OPA1
MIM	Mitochondrial inner membrane
MOM	Mitochondrial outer membrane
mRNA	Messenger RNA
MS	Mass spectrometry
MSMS	Tandem mass spectrometry
mtDNA	Mitochondrial DNA
MTG	Mitotracker green
NADH	Reduced form of Nicotinamide adenine dinucleotide
Nano-LC	Nano-flow liquid-chromatography
ND2	NADH-ubiquinone oxidoreductase chain 2
Ndufv1	NADH dehydrogenase [ubiquinone] flavoprotein 1, mitochondrial
NRF-1	Nuclear respiratory factor -1
NTC	None-template control
OPA1	Optic atrophy protein 1
OxPhos	Oxidative phosphorylation
PBS	Phosphate buffered saline
PCR	Polymerase chain reaction
PDHA1	Pyruvate dehydrogenase alpha 1

PFA	Paraformaldehyde
PFK	Phosphofructokinase
PGC-1α	Peroxisome proliferator-activated receptor gamma coactivator 1-alpha
PGC-1β	Peroxisome proliferator-activated receptor gamma coactivator 1-beta
PKM2	Pyruvate kinase M2
PMSF	Phenylmethylsulfonylfluorid
PPAR	Peroxisome proliferator-activated receptors
PRC	PGC-1-related coactivator
Ptc	Patched (drosophila)
PTCH	Patched (mammals)
PVDF	Polyvinylidene fluoride
qPCR	Quantitative PCR
RCD	Respiratory chain diseases
RNA	Ribonucleic acid
RNAi	RNA interference
ROS	Reactive oxygen species
rRNA	Ribosomal RNA
SAG	Smoothened Agonist
SANT	Smoothened Antagonist
SDS	Sodium dodecyl sulphate
SDS-PAGE	Sodium dodecyl sulphate – polyacrylamide gel electrophoresis
SHH	Sonic hedgehog
Ski	Skinny hedgehog
Smo	Smoothened (mouse/drosophila)
SMOH	Smoothened (humans)
SSC	Side scatter
Su(Fu)	Suppressor of Fu (Drosophila)
SUFU	Suppressor of Fu (Mammals)
TBS-T	TBS/Tween 20
TCA cycle	Tricarboxylic acid cycle
TEM	Transmission electron microscopes
TEMED	N,N,N',N'-Tetramethylethylendiamine
TFAM	Mitochondrial transcription factor A
TFB1M/ TFB2M	Mitochondrial transcription factor B1/B2
TFE	2,2,2-trifluoroethanol
TMRE	Tetramethylrhodamine,ethyl ester
TNF-α	Tumor necrosis factor alpha
TOF	Time Of Flight
Tomm20	Mitochondrial import receptor subunit TOM20 homolog
tRNA	Transfer RNA
TZD	Troglitazone
UCP-1	Uncoupling protein 1
WAT	White adipose tissue
WHO	World health organization
YY1	Transcriptional repressor protein YY1
β-ME	2-Mercapto Ethanol

1. INTRODUCTION

1.1 Mitochondria

Mitochondria are semi-autonomous organelles derived from a symbiosis between aerobic bacteria and primordial eukaryotes[1]. Mitochondria contain their own genome, they are equipped with their own protein synthesis machinery, and they are key organelles playing an important role in controlling the life and death of cells since they produce the vast majority of the cells adenosine triphosphate (ATP) via oxidative phosphorylation (OxPhos). For this, oxygen is transported by erythrocytes, and taken up by the cells to be used in the mitochondria to generate ATP. Besides their essential function to synthesize ATP many catabolic and anabolic reactions take place in mitochondria. Among others, the citric acid cycle, the β-oxidation of fatty acids and the conversion of pyruvate to the general building block acetyl-CoA take place in the mitochondrial matrix. Furthermore, mitochondria contribute to intracellular signalling pathways via the generation of reactive oxygen species (ROS) and Ca^{2+} release. In addition, they are important regulators of apoptosis pathways. Thus, mitochondria are indispensible for life, even in anaerobic organisms.

1.1.1 Electron transport chain and oxidative phosphorylation

The ability of mitochondria to produce ATP relies on five inner mitochondrial membrane complexes that oxidize the products of glycolysis and lipolysis: NADH and $FADH_2$. They transfer electrons to molecular oxygen and pump H^+ protons across the membrane. This establishes an electrochemical gradient that drives the phosphorylation of ADP to ATP. In the first complex (NADH Dehydrogenase) two electrons of the donor NADH are transferred to a lipid-soluble carrier, ubiquinone. Complex II (Succinate Dehydrogenase) provides additionally electrons for ubiquinone. Electrons are further transported to Complex III (Cytochrome bc1 complex) where they are transferred to two molecules of cytochrome C, a water-soluble electron carrier located within the intermembrane space. Four electrons are then removed from four molecules of cytochrome C by complex IV (Cytochrome C oxidase) and transferred to the final acceptor molecular oxygen, producing two molecules of water.

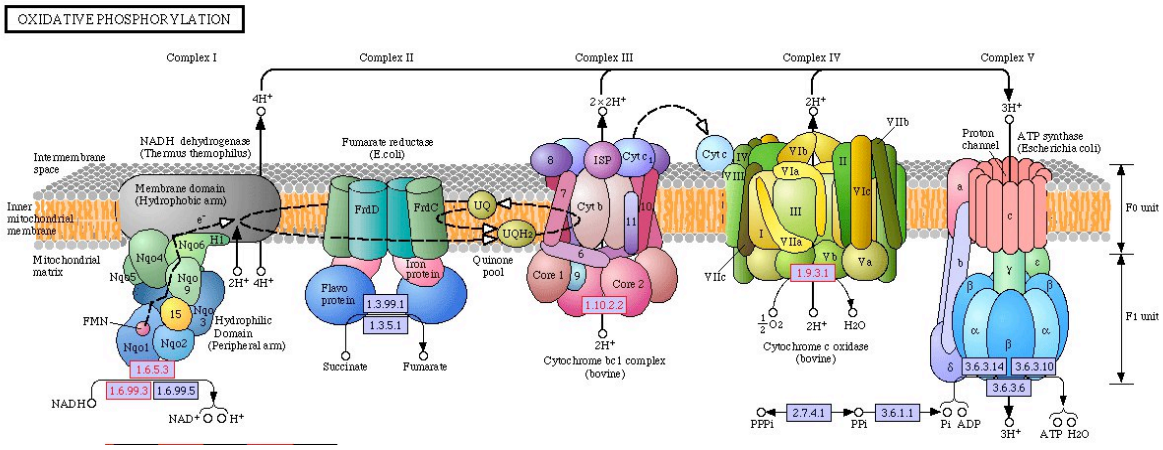

Figure 1 The electron transport chain (ETC) in the inner mitochondrial membrane (source: http://www.genome.jp/kegg/)

Complex I, III and IV are also proton pumps which couple their chemical reactions to the establishment of the proton gradient across the inner mitochondrial membrane, with the inside of the inner mitochondrial membrane being more negative than the outside. The resulting proton gradient is used to synthesize ATP through the ATP Synthase (Complex V).

The term *coupled respiration* was first proposed by Peter D. Mitchell (Nobel Prize in Chemistry 1978)[2], and describes the dependence of the uptake of oxygen by mitochondria on the simultaneous conversion of ADP and phosphate to ATP. The coupling of respiration and phosphorylation can be broken by mechanical or osmotic disruption of the mitochondria. Moreover there are uncoupling agents, like carbonyl cyanide-p-trifluoro-methoxy-phenylhydrazone (FCCP) and carbonyl cyanide m-chloro phenyl hydrazone (CCCP), which lead to rapid respiration without concomitant ATP synthesis – they uncouple respiration from phosphorylation. There is even a physiological state where exposure to cold leads to uncoupling of mitochondria in brown adipose tissue (BAT). In this state the mitochondrial proton gradient is used to generate heat instead of ATP[3].

1.1.2 Mitochondrial biogenesis and dynamics

As mentioned before mitochondria have such a diverse repertoire of bioenergetic and metabolic functions. Thus it comes with no surprise that mitochondrial mass, function and morphology differ significantly in different cell types. For instance there is a difference in number of mitochondria in tissues with high energy demand (for instance cardiomyocytes) and in tissues with low energy demand (white adipose

tissue). Another example is the specialized function of mitochondria in different tissues (e.g. steroid synthesis in adrenal gland or cholesterol in liver). Moreover mitochondrial biogenesis is dynamically regulated in response to physiological cues such as physical activity and nutrient availability fitting the needs of different physiological states.

Of note, mitochondria are not generated de novo. They propagate by growth and division (also know as mitochondrial fission) of already existing mitochondria. Actually mitochondria are very dynamic organelles that are in a constant flux, driven by continuous fusion and fission. The balance between these two processes determines the shape of mitochondria in a cell. If there is for instance a shift towards fusion, this will lead to the generation of interconnected elongated mitochondria[4,5,6,7]. A shift towards fission on the other hand will result in fragmented mitochondria[8, 9]. The molecular players on the fusion side are the so called mitofusins. These are GTPases localized on the outer membrane of mitochondria. In mammals we can find two mitofusin genes, namely Mfn1 and Mfn2, mediating the fusion process of mitochondria[10]. Another protein essential for mitochondrial fusion is the GTPase OPA1 (optic atrophy protein 1), which is located in the intermembrane space. Together, mitofusins and OPA1 promote mitochondrial fusion. This is supported by some findings. For instance mutant cells comprise fragmented mitochondria in yeast[11, 9, 12] and mammals[13, 8]. If cells lacking mitofusins or OPA1 are fused, their mitochondria are not able to mix their matrix content[14, 8]. Moreover, isolated mitochondria from yeast mutants lacking Fzo1 or Mgm1 (Mitofusin- and OPA1 orthologues, respectively) do not show the ability to fuse in vitro[15, 16].

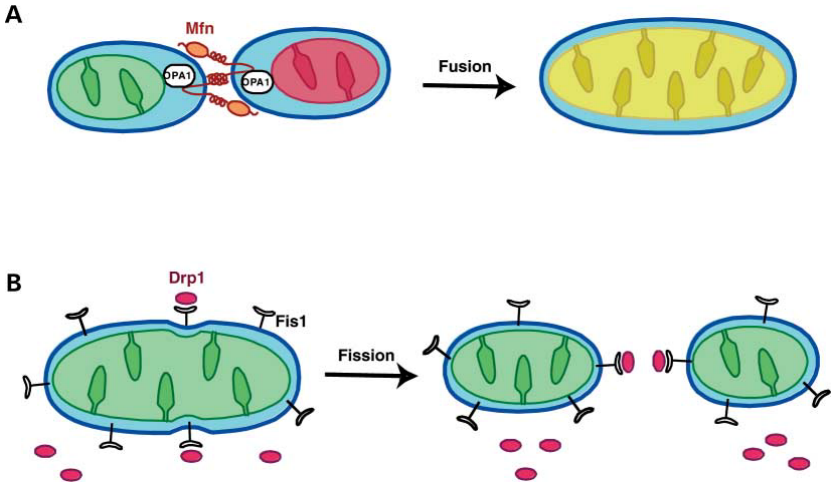

Figure 2 Mitochondrial fusion and fission machinery (reviewed in *Human Molecular Genetics* **14**, 283-289 (2005))

The main players on the fission side are dynamin-related protein Drp1[7] and Fis1. The GTPase Drp1 localizes to discrete spots on mitochondria, some of them mark sites for future fission. In Yeast Dnm1 (the Drp1 ortholog) recruitment to the mitochondrial membrane mainly relies on the protein Fis1 and two adapter proteins[17, 18, 19, 20]. Yeast Fis1 mutants show a strong decrease of Dnm1 localization to mitochondria[21, 22]. However RNAi knockdown of Fis1 in mammalian cells did not interfere with the localization of Drp1[23]. As expected, cells lacking Drp1 or Dnm1 show a shift towards fusion resulting in highly interconnected mitochondrial nets[24, 25]. A disruption of the balance of these two processes has an impact on two key functions of mitochondria, namely electron transport and regulation of apoptosis. Mfn-null cells and cells depleted of OPA1 by RNAi show reduced respiration rates in both endogenous and uncoupled respiration[26]. It has been suggested that Drp1 plays a role in apoptosis since dominant-negative Drp1 and Drp1-RNAi inhibit fragmentation of mitochondria during apoptosis and further diminish cell death[27].

Fusion of mitochondria also implicates, besides the mixing of membranes, the mixing of the mitochondrial genetic material. The mitochondrial DNA (mtDNA) is organized into separate units called nucleoids. Each mitochondrion is equipped with several nucleoids comprising multiple mtDNA genomes. A closer look at the mitochondrial genome shows that only 13 proteins are encoded and additionally 2 rRNAs and 22 tRNAs for translation within the organelle. These 13 proteins encode for subunits of complex I, III, IV and V of the electron transport chain. As a matter of fact, these 13 proteins are not sufficient to make up a whole mitochondrion. Thus the vast majority of genes encoding for the 1100-1500 proteins of the mitochondrial proteome are nuclear genes[28]. Therefore a coordinated transcription of mitochondrial genes in the nucleus and mitochondria is mandatory. In view of this it is obvious that mitochondrial biogenesis is a very complex process, which requires the synthesis, import, and incorporation of proteins and lipids to the existing mitochondrial compartments as well as replication of mtDNA.

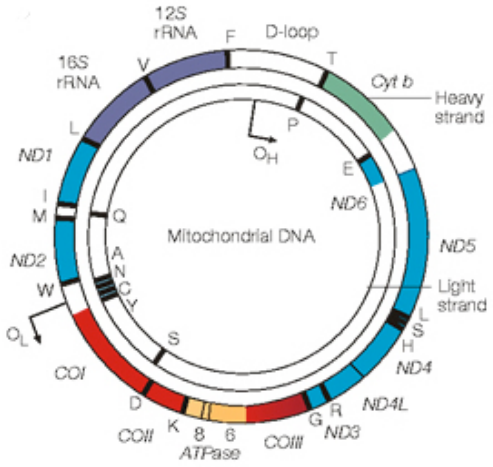

Figure 3 mtDNA (reviewed in *Nature Reviews Genetics* **6**, 389-402 (May 2005))

This dual genetic control is achieved by nucleus-encoded mitochondrial proteins that control the transcription and replication of mtDNA, i.e. mitochondrial transcription factor A (TFAM) and mitochondrial transcription factor B1/B2 (TFB1M/ TFB2M)[29,30,31]. These proteins are required for initiation of transcription by mitochondrial RNA polymerase and are induced in response to signals promoting mitochondrial biogenesis. Since mitochondrial biogenesis is a long-term adaptive response, there is also a need to fulfil transient changes in energy demands. This is enabled by changes in expression of a subset of mitochondrial genes of critical regulators and by the enhancement of mitochondrial function. Moreover there is also the need for differential expression of a subset of mitochondrial genes in different tissues due to the specialized function of mitochondria in certain tissues. It has been observed that about 50% of mitochondrial gene expression is tissue-specific[32]. One prominent example might be the cholesterol synthesis in liver tissue. Examples for such transcriptional regulators of mitochondrial biogenesis and function are nuclear respiratory factor -1 (NRF-1) and GA-binding protein (GABP or NRF-2). They are nuclear DNA-binding factors regulating transcription of OxPhos and mitochondrial transcription/import genes.

It seems that endogenous NRF-1 is constitutively active, since silencing of NRF-1 significantly suppresses mitochondrial target genes[33,34,35]. Activity of the NRF-1 protein can be modulated by phosphorylation and/or interactions with PGC-1α, PGC-1β, PRC and cyclin D1[31,36,37,38,39]. NRF-1 expression itself is regulated by two major signals: increases in Ca2+ levels and AMP-activated protein kinase (AMPK) activation. Induction of NRF-1 expression could be observed in vivo in muscle of rat and zebra

fish by exercise[40,41,42]. This induction due to exercise has not been seen in human studies so far. In muscle of rats NRF-1 expression could also be induced when feeding them with a creatine analog that activates AMPK provoking changes similar to those induced by exercise training[43].

GABP was first identified as an activator of the Cox IV promoter[44]. Later it was shown that a knockdown of GABPα (one of the two subunits in the GABP heterotetramer and responsible for DNA-binding) expression reduces the expression of all 10 nuclear-encoded Cox genes as well as Tfam, Tfb1m, and Tomm20 (a component of the import machinery). This resulted in a 20% decrease in cellular COX activity[45]. Like NRF-1, GABP is also expressed broadly and is regulated by developmental and physiological signals. Another example is the family of peroxisome proliferator-activated receptors (PPARs), which are nuclear receptors that regulate genes involved in lipid transport and metabolism in response to fatty-acid derived ligands. Furthermore, there is the family of estrogen-related receptors (ERR) and some other nuclear transcription factors (CREB, c-myc, YY1) modulating the mitochondrial program.

1.1.3 Mitochondria in disease

Inheritance of mtDNA is different from Mendelian genetics in almost every aspect. First of all, the mitochondrial genome consists of a multicopy circular dsDNA molecule (16.6 kb in humans). This leads to an important feature of mitochondrial genetics, homoplasmy and heteroplasmy[46]. Homoplasmy is when all copies of the mitochondrial genome are identical, whereas heteroplasmy is when there is a mixture of two or more mitochondrial genotypes[46].

Clinical features of mtDNA diseases are that they affect many tissues. Furthermore, they are presenting with highly variable symptoms, which makes diagnosis difficult. Since mitochondria generate the vast majority of cellular ATP through oxidative phosphorylation it is apparent that respiratory chain diseases (RCD) represent a large subset of mitochondrial disorders. Defects in this essential machinery can cause diseases ranging from neonatal lethality to adult-onset neurodegeneration[53]. There has been estimations suggesting that about 15-20% of RCD are due to mtDNA mutations, while the rest are caused by nuclear defects[47,48]. Kirby et al.[49] described, for the 92 protein-encoding genes whose mutations underlie RCD, five critical pathways. First, mutations in any of the 13 mtDNA protein encoding-genes (or in any

of its tRNAs or rRNAs) can underlie RCDs[50,51,52]. Moreover, RCDs can be caused by mutations in many of the nuclear genes encoding these subunits. Furthermore, mutations in genes encoding for the proper import, maturation and assembly of the OxPhos complexes can give rise to RCDs. In addition, mitochondrial membrane dynamics are required for a proper import. A balanced pool of nucleotides for proper replication and transcription is essential and mutations in these pathways can also cause RCDs[53].

1.2 The Hedgehog signalling pathway

The hedgehog (Hh) protein family compromises secreted signalling proteins that play a crucial role in many developmental processes conserved from Drosophila to humans. In 1980 Nüsslein-Volhard and Wieschaus performed a large-scale screen for mutations that impair the development of the fruit fly larval body plan, thereby identifying mutations in the Hh gene. The phenotype resulting from this mutation – the short and "spiked" appearance of the cuticle of the Drosophila larvae – gave the protein the name. These proteins control cell growth, survival and fate, and therefore act as a regulator of proliferation, differentiation and pattern formation during embryogenesis and organogenesis. Aberrant activation of this pathway has been linked to multiple types of cancer.

1.2.1 The hedgehog protein family

Hedgehog proteins are highly hydrophobic proteins. After they have been secreted they can diffuse and establish gradients in tissues, acting as morphogens, which is crucial for the proper embryonic development[54]. Hedgehog acts in a time- and dose-dependent manner both directly and indirectly, both over a short and long range. Thus altering the amount but also the time of hedgehog exposure seems to significantly influence intracellular signalling[55,56,57].

As already stated before, components and mechanisms for hedgehog processing and secretion are highly conserved from flies to humans. There has been an expansion of hedgehog genes as a result of the vertebrate genome duplication[58]. Hence, three hedgehog homologues can be found in humans that show different spatial and temporal distribution patterns: Sonic hedgehog (SHH), Indian hedgehog (IHH) and

Desert hedgehog (DHH)[59]. DHH is the one that is most closely related to Drosophila hedgehog whereas SHH and IHH are more closely related to each other[54,60,61,62].

The expression of DHH is largely restricted to gonads, including sertoli cells in the testis and granulosa cells of ovaries. DHH-deficient mice do not show notable phenotypes in most tissues and are viable. In contrast to females, males are infertile due to complete absence of mature sperm[61]. IHH is expressed in a limited number of tissues, including primitive endoderm, gut and prehypertrophic chondrocytes in the growth plates of bones. Approximately 50% of IHH$^{-/-}$ embryos die during early embryogenesis due to poor development of yolk-sac vasculature[61]. SHH is the most widely expressed Hedgehog signalling molecule in humans. It is expressed during early vertebrate embryogenesis in the midline tissue where it controls the patterning of the left-right and dorso-ventral axes of the embryo[63,64,65,66,67]. During organogenesis, i.e. later in development, SHH is expressed in most epithelial tissues. Deletion of SHH leads to cyclopia, defects in ventral neural tube, severe distal limb malformation, absence of vertebra and most of the ribs, as well as failure of lung branching[61].

1.2.2 Hedgehog processing

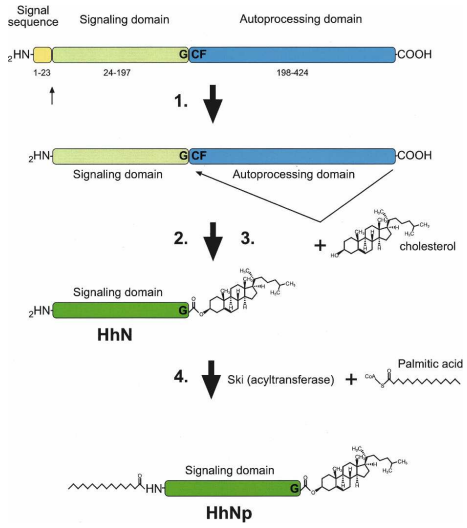

Figure 4 Hedgehog processing (reviewed in Genes & Development 22, 2454-2472, 2008)

The generation of an active Hh ligand in the producing cell requires the processing of the precursor protein. The first step in processing is the cleavage of the signal sequence. Next an autocatalytic cleavage between conserved glycine and cystein

residues occurs[68], releasing the ~19kDa N-terminal Hh signalling domain (HhN) that contains a cholesterol modified C terminus[69]. Due to this cholesterol modification HhN can now associate with the plasma membrane, leading to the addition of a palmitic acid moiety at the N terminus of HhN by the acyltransferase Skinny hedgehog (Ski in Drosophila, HHAT in humans) resulting in the fully active HhNp protein[70].

1.2.3 The hedgehog signalling components

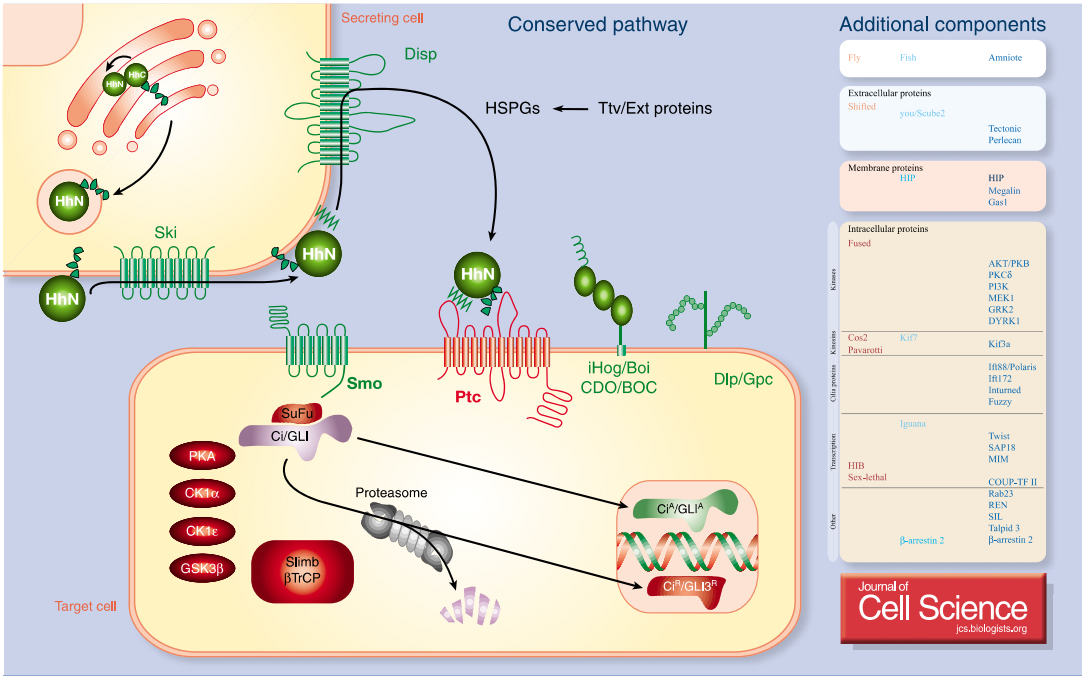

Figure 5 Hedgehog Signalling (reviewed in Journal of Cell Science 120 (1), 3-5, 2007)

After translation Hedgehog gets processed before it can be secreted. Hedgehog producing cells require the twelve pass transmembrane transporter-like protein Dispatched (DISP) to release cholesterol-modified Hh to the extracellular space[71]. In consequence, a loss of DISP function will lead to an accumulation of Hh in the producing cell and furthermore diminish target gene expression in responding cells[54,60,62,72]. In humans there are three dispatched homologues (DISP1-3), whereas in mice only two dispatched homologues (mDISPA & mDISPB) could be identified[73]. Subsequent transport of Hh through tissues apparently require heparan sulfate, since embryos lacking heparan sulfate-synthesizing enzymes of the EXT/tout velu (ttv) family are not able to transport Hedgehog[74,75]. On the responding cell two classes of accessory receptors facilitate binding of Hedgehog to its signalling receptor patched 1

(PTCH1 in humans, Ptch1 in mouse, Ptc in Drosophila): the glypican-family of cell surface proteoglycans and the transmembrane proteins iHog and Boi (CDO and BOC in vertebrates)[76,77,78]. In the absence of Hedgehog, Ptc catalytically inhibits the activity of the seven-transmembrane-span receptor-like protein Smoothened (SMOH in humans, Smo in mouse/Drosophila)[79]. Binding of Hedgehog to Ptc results in loss of Ptc activity, therefore activating Smo that is now able to transduce the Hedgehog signal to the cytoplasm ultimately resulting in the activation of the Ci/GLI family transcription factors[79,80,81,82].

The major difference between Drosophila and mammals in hedgehog signalling seems to be how the intracellular signal is conveyed. First of all, there seems to be a difference how Smo localization is regulated. Whereas in Drosophila Smo accumulates at the cell surface after Hh stimulation[83], mammalian Smo is internalized[84]. Furthermore, Drosophila Smo activation is coupled to the hyperphosphorylation of 26 serine/threonine residues that are not conserved in mammals [60]. Another difference can be found at the level of transcriptional control by the Ci/GLI transcription factor. In the absence of Hedgehog in Drosophila full length Ci is retained in the cytoplasm by Costal2 (Cos2) and suppressor of Fused (Su(Fu)). In addition Ci phosphorylation is promoted by Cos2, leading to processing of Ci in the proteasome that results in the formation of the repressor form Ci^{R} [60]. After binding of Hh, Smo is activated, leading to an enhanced binding of Cos2 to Smo. Now Cos2 is not able to trigger Ci processing, leaving Ci in a transcriptional active form (Ci^{A}) that can enter the nucleus and activate its target genes[81].

Mammals differ from Drosophila in that they have divided the activities of Ci to three Ci homologues, namely GLI1, GLI2 and GLI3[72]. With GLI1 being a strong transcriptional activator and its expression being dependent on GLI2 and/or GLI3-mediated transcription. Therefore GLI1 expression can be used as a suitable readout for activation of classical HH pathway activation[85]. Although GLI2 and GLI3 both contain activator and repressor domains, it is GLI2 that primarily acts as an activator whereas GLI3 mainly represses target gene expression[72]. Furthermore mouse Smo is not stabilized after pathway activation by Shh and it does not bind any of the two Cos2 orthologs (Kif27, Kif7)[60]. It seems to be that Su(Fu) is the component in mammals that suppresses the pathway in the absence of ligand, since loss of Su(Fu) leads to complete activation of the Hh pathway in mouse embryos[86].

There are several small-molecule modulators of the Hedgehog pathway – some of them are synthetic, some of them occur naturally. Probably the most famous one is the plant steroidal alkaloid cyclopamine, which inhibits the pathway by direct binding to Smo[87]. Since there is a structural similarity between cyclopamine and sterols, it has been suggested that endogenous sterols might play a role in regulating Smo activity[88]. Endogenous metabolites that might exert this function are oxysterol and vitamine D3 derivates[89,90]. Other Smo-binding antagonists are for instance SANT1-4 (Smoothened Antagonist 1-4)[91] and GDC-0449[92]. Downstream inhibition of Hh target genes can be achieved by GANT58 and GANT61, two inhibitors of Gli activities[92]. In contrast to these hedgehog signalling antagonists the Smo binding chemical SAG (Smoothened Agonist) represents a widely used potent activator of canonical hedgehog signalling[93].

1.2.4 Mammalian hedgehog at the primary cilium

Yet another characteristic solely found in mammalian Hh signalling is the formation of the primary cilium. Evidence for that comes from findings that mutation in components required for the formation of the primary cilium, lead to embryonic phenotypes resembling the loss of Shh signalling[94]. This is further strengthened by findings that the loss of orthologs of cilia proteins does not affect Hh signalling in Drosophila or Zebrafish[95,96]. In mammals Su(Fu) and unprocessed GLI proteins are localized to the distal tip of the primary cilium[97], and upon activation of the Hh pathway Smo is recruited to the distal tip of the primary cilium as well[98]. In the absence of Hh ligands PTCH1 – localized at the base of the primary cilium – prevents Smo translocation to the tip of the cilium, thus preventing pathway activation[99].

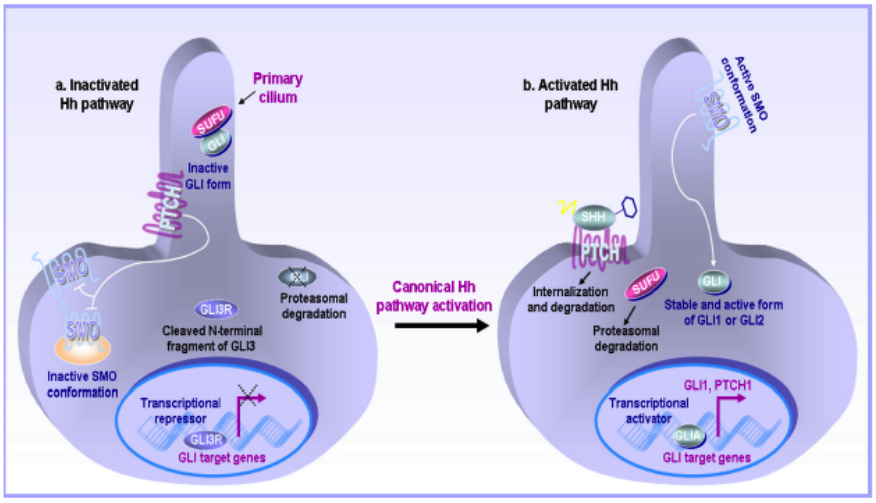

Figure 6 Primary cilium in the mammalian Hedgehog pathway (reviewed in Pharmaco. Rev. 62 (3) 497-524, 2010)

1.3 Obesity

The world health organization (WHO) defines overweight and obesity as a disease in which abnormal or excessive fat accumulation in adipose tissue and other organs presents a risk to health. A classification that is commonly used is the body mass index (BMI, i.e. the body weight in kg divided by the height in meters squared (kg/m^2). A BMI equal to or greater than 25 kg/m^2 is defined as overweight, equal or greater than 30 kg/m^2 is defined as obese[100]. Looking at the numbers, obesity is a growing epidemic. In 2008 the WHO estimated that about 1.5 billion adults aged 20 years and older were overweight. In 2010 an alarming number of more than 40 million children under the age of five were classified as overweight[101]. Moreover, the prevalence of childhood obesity has tripled in the past 30 years[102]. Common health consequences of a raised BMI are cardiovascular disease, diabetes, musculoskeletal disorders, some cancers and a reduced life expectancy.

1.3.1 Adipose tissue

We can distinguish between two adipose tissues: brown (BAT) and white adipose tissue (WAT), with the first one solely found in mammals. Differences between these two tissues are that only BAT expresses uncoupling protein 1 (UCP-1) in order to produce heat at the expense of ATP. Furthermore, brown adipocytes contain multiple small lipid droplets and are filled with numerous heat generating mitochondria[103]. One particular feature of WAT is the storage of energy in the form of triglycerides in lipid droplets[104]. Furthermore white adipocytes secrete factors, known as adipokines (e.g. Leptin, Adiponectin), conferring them with an endocrine function regulating fat mass and nutrient homeostasis. In addition, white fat cells are involved in the regulation of the immune response, blood pressure, haemostasis, bone mass and reproductive function[103]. Of note, obese people display a severe imbalance in this adipokine network system that contributes to an impaired adipocyte metabolism.

1.3.2 Obesity and metabolic disorders

In 1993 Hotamisligil et al. were the first to describe obesity state as a state of "low-grade systemic inflammation"[105]. The excess consumption of nutrients is a metabolic trigger for inflammation, though different to classical inflammation[102]. Inflamed obese tissue shows an increase in number (hyperplasia) and size (hypertrophy) of

adipocytes[104], and moreover increased levels of cytokines, e.g. TNF-α[106], IL-6, IL-1β, CCL2 and others. In addition, there is an increased infiltration of immune cells, for instance macrophages, into the adipose, which also contributes to the increased tissue cytokine expression[107,108]. This all together results in an enhanced lipolysis in adipocytes, which further leads to more free fatty acids (FFA) being released. It has been suggested that the release of adipose FFA leads to increased FFA uptake in skeletal muscles and liver (Figure 7). The concomitant increased secretion of insulin by pancreatic β-cells reprograms whole body nutrient distribution. Over time the combination of increased levels of insulin, FFA and pro-inflammatory cytokines leads to systemic insulin resistance and pancreatic β-cell failure, and thus to the development of Type 2 diabetes[109].

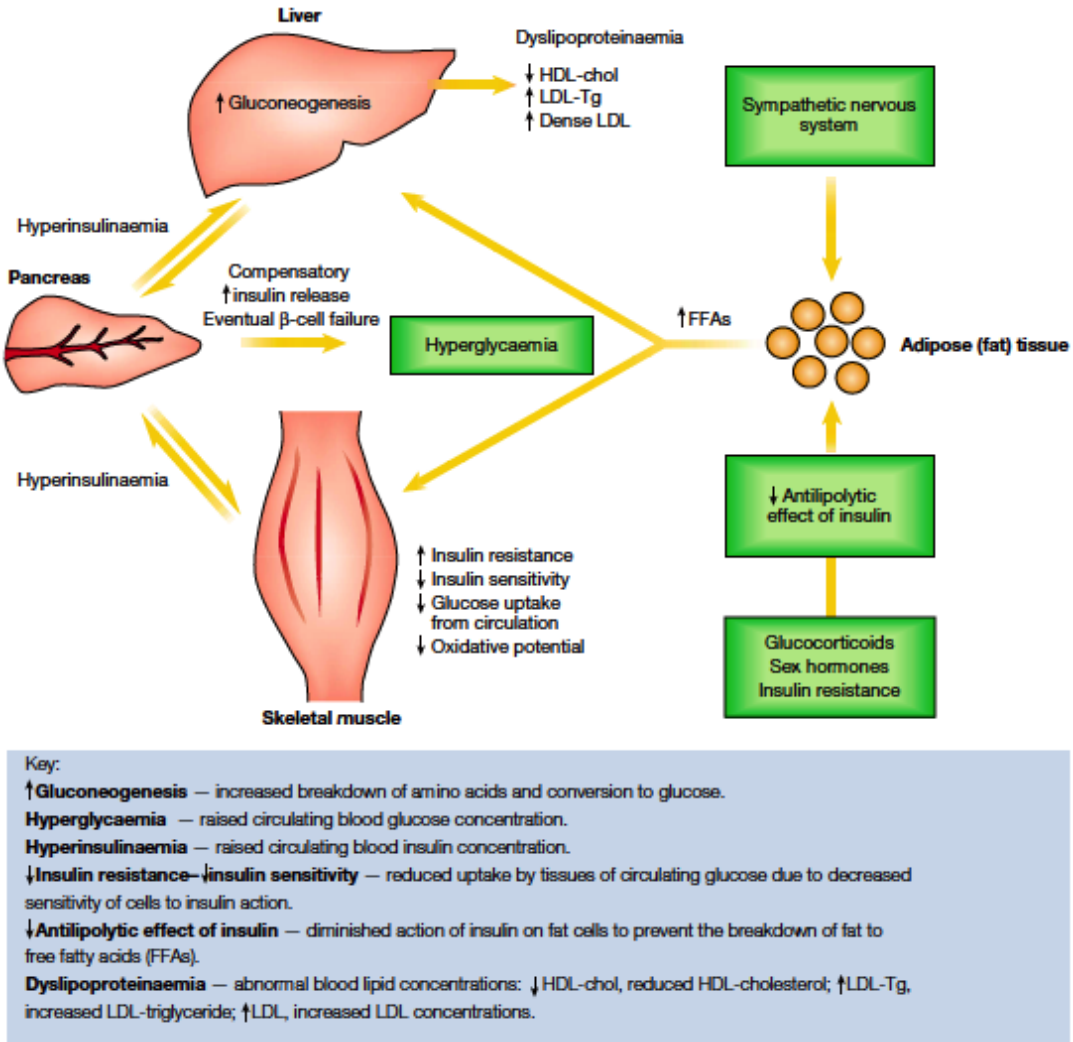

Figure 7 Obesity and type 2 diabetes (reviewed in Nature 404, 635-643, 2000)

2. PROBLEM DEFINITION AND OBJECTIVE

Obesity is now a global epidemic, with over 200 million men and 300 million women being obese, exposing them to risk for many diseases like diabetes, hypertension, heart disease, sleep apnoea and cancer[110].

Hedgehog is primarily known for its fundamental function in development processes and for causing cancer as a result of an aberrant activation in adults. Recently, Hedgehog has been identified as a determinant for brown versus white adipose cell fate, blocking white adipocyte differentiation in vitro and in vivo[111]. Knock out mice with a fat-specific activation of the Hedgehog signalling pathway showed a massive loss of the white adipose tissue, whereas the development of brown adipose tissue was unaffected. Furthermore, these mice showed normal glucose tolerance and insulin sensitivity. Based on this we started to investigate the effects of Hedgehog signalling on mature adipocytes. First, we observed a colour change in the media of 3T3-L1 mature adipocytes after a 48 hours exposure to the potent smoothened agonist SAG. After making sure that this change was not due to a bacterial infection, we started to investigate this phenomenon in more detail and figured out that SAG stimulated adipocytes show an increased glucose consumption rate and an increased lactate production rate. To gain further insight into this hedgehog induced metabolic shift we performed a genome wide gene expression analysis coupled to a quantitative proteomic approach. Interestingly, both approaches revealed that Hedgehog stimulated adipocytes display a metabolic signature closely resembling the Warburg effect in cancer cells[112]. Furthermore we could identify new Hedgehog targets and mechanisms in mature adipocytes. We could observe an increased glucose uptake and glycolysis, with glycolytic key enzymes being significantly altered in Hedgehog treated adipocytes, namely phosphofructokinase (PFK), pyruvate kinase M2 (PKM2) and pyruvate dehydrogenase alpha 1 (PDHA1). These changes led to a shift towards lactate production. Furthermore, we noticed a decrease in other metabolic processes like fatty acid synthesis, fatty acid oxidation, oxidative phosphorylation and a reduced TCA entry of pyruvate. Based on our previous data, i.e. the observed changes in glycolysis and substrate flux into mitochondria, the main objective of this diploma thesis was to address whether Hedgehog signalling impacts mitochondrial structure and function in mouse 3T3-L1 adipocytes.

This objective was addressed by the following specific aims:

- Establishment of a mitochondrial proteomic approach for the evaluation of differences in the mitochondrial proteome following Hedgehog stimulation
- Investigation of mitochondrial dynamics by qPCR of mitochondrial fusion and fission targets following Hedgehog treatment
- Evaluation of effects of Hedgehog on mitochondrial biogenesis and distribution by FACS analysis and confocal microscopy using Mitotracker Green FM
- Determination of the mitochondrial membrane potential upon Hedgehog stimulation by FACS analysis and confocal „live“ cell imaging with the membrane potential sensitive dye TMRE
- Exploration of the effects of Hedgehog stimulation on the ultrastructure of mitochondria by electron microscopy

3. MATERIALS AND METHODS

3.1 Cell culture

3.1.1 Reagents and solutions

Calf Serum (CS)	PAA
3-isobutyl-1-methylxanthine (IBMX)	Sigma
Dexamethasone (DEX)	Sigma
DMEM high glucose (4.5 g/L)	PAA
Fetal Bovine Serum HI (FBS, heat inactivated)	PAA
Gentamycin (50 mg/mL)	Gibco
Insulin	Sigma
PBS 1X	Sigma
Smoothed Agonist (SAG)	Alexis
Troglitazone (TZD)	Sigma
Trypsin/EDTA 1X 0.05%/0.02% in PBS	PAA

3.1.2 Procedure

3T3-L1 cell line handling and adipocyte differentiation

Murine 3T3-L1 preadipocytes were obtained from ATCC (American type culture collection). They were routinely cultured in Dulbecco's modified eagle's medium (DMEM) supplemented with bovine calf serum (10%, v/v) and gentamycin (50 μg/ml). Every 2 to 3 days 3T3-L1 cells were subcultured, ensuring not to reach confluence. For differentiation, preadipocytes were subcultured in different culture plates respective to each experiment and grown to confluence. Cells were cultured for an additional 48 hours after reaching confluence and then induced to differentiate by exposing them to an adipogenic induction medium (this time point was designated as day 0). This media consists of the growth media (DMEM, 10% FBS) supplemented with 1.0 μM dexamethasone, 0.25 mM IBMX, 1.74 μM insulin and 5 μM Troglitazone. On day 2 the induction medium was replaced by adipocyte differentiation medium consisting of growth medium complemented with 1.74 μM insulin and 5 μM Troglitazone. After 2 days exposed to adipocyte differentiation media, cells were exposed to normal growth media and exchanged every other day for the duration of the experiment.

SAG Treatment

Both subconfluent preadipocytes (~80% confluency) and adipocytes at day 5 of differentiation were starved for 18 h in DMEM supplemented with bovine serum albumin (BSA, 1%, weight/volume). After cells were synchronized by starvation they were treated with 200 nM Smoothened agonist (SAG) or control vehicle for 24 and 48 hours.

3.2 Sample preparation

3.2.1 Reagents and solutions

Ethylenediaminetetraacetic acid (EDTA)	Sigma
Magnesium chloride ($MgCl_2$)	Sigma
PBS 1X	Sigma
Phenylmethylsulfonylfluorid (PMSF)	Sigma
Potassium chloride (KCl)	Merck
Proteinase Inhibitor IC 25X	GE Healthcare
Sodium chloride (NaCl)	Sigma
Sodium deoxycholate	Sigma
Sodium dodecyl sulfate (SDS)	Sigma
Sucrose	Sigma
Tris	Gerbu

	Stock	**Final concentration**	**V_E = 15 ml**
Solution A*	1 M Tris HCl pH 7.6	10 mM Tris HCl pH 7.6	150 µl
	1 M KCl	10 mM KCl	150 µl
	1 M $MgCl_2$	15 mM $MgCl_2$	225 µl
Solution B	2 M Sucrose	2 M Sucrose	
Solution C*	2 M Sucrose	0.25 M Sucrose	1875 µl
	1 M Tris HCl pH 7.6	10 mM Tris HCl pH 7.6	150 µl
	1 M $MgCl_2$	$1.5x10^{-4}$ M $MgCl_2$	2.25 µl
Solution D*	2 M Sucrose	0.25 M Sucrose	1875 µl
	1 M Tris HCl pH 7.6	10 mM Tris HCl pH 7.6	150 µl
	0.5 M EDTA-NaOH pH 8	10 mM EDTA-NaOH pH 8	300 µl

	Stock	**Final concentration**	**V_E=250 ml**
RIPA buffer	1 M Tris-HCl pH 7.6	50 mM Tris-HCl pH 7.6	12.5 ml
	5 M NaCl	150 mM NaCl	7.5 ml
	0.5 M EDTA	1 mM EDTA	0.5 ml
	10% Sodium deoxycholate	1% Sodium deoxycholate	2.5 g
	20% SDS	0.1% SDS	1.25 ml
	0.1 M PMSF	1 mM PMSF	Prior to use
	Proteinase Inhibitor IC 25X		Prior to use

* solutions are prepared freshly on the day of use from stock solutions

3.2.2 Procedure

3.2.2.1 Mitochondria isolation for proteomic analysis

The preparation started from a cell layer of treated 3T3-L1 adipocytes. Immediately after cells were taken out of the incubator they were placed on ice to prevent degradation of proteins. The cells were washed with ice cold PBS to get rid of all the media. Then 1 ml hypotonic solution A was added to the cell layer and cells were thoroughly scraped of the flask, homogenized with an Eppendorf P1000 and transferred to a 15 ml tube. To ensure sufficient yield of isolated mitochondria, two 150 cm^2 flasks were pooled together at this step to represent one biological sample. Next to swell the cells, they were incubated on ice for 15 minutes. $1/7^{th}$ of volume solution B was added to the cell suspension, shortly vortexed, incubated another minute on ice and then passed 10 times through a G25 needle. This homogenate then was centrifuged at 1200 g for 5 minutes at 4°C to get rid of unbroken cell, debris and nuclei (Beckman Coulter Allegra X-12R Centrifuge). The supernatant after this low speed centrifugation step then was centrifuged at 8000 g for 10 minutes at 4°C to pellet the mitochondria (Thermo Scientific Sorvall RC6+ Centrifuge). The mitochondrial pellet was resuspended in solution C and low speed and high speed centrifugation steps were repeated as stated before. Another wash step was performed by resuspending the mitochondrial pellet in solution D. Again low speed and high speed centrifugation steps were repeated as stated before. The final mitochondrial pellet was either shock frozen in liquid nitrogen and stored at -80°C until use or instantaneous processed as mentioned in 3.3.1.2.

3.2.2.2 Western blot samples

As cells were taken out of the incubator, they were immediately placed on ice to prevent protein degradation. Next cells were washed two times with ice cold PBS and scraped with RIPA buffer (100 µl/well) and instantaneous snap frozen in liquid nitrogen and stored on -80°C. The next day lysates were thawed under constant rolling for 1 hour at 4°C, then centrifuged full speed for 30 minutes at 4°C, and finally supernatants were transferred to a new tube. Protein concentration was determined using the Bradford method and samples were either instantly processed or again snap frozen in liquid nitrogen and stored on -80°C until use.

3.3 Proteomic analysis

3.3.1 1D-GeLC/MSMS

In the 1D-PAGE approach proteins are separated solely by their molecular mass. Therefore proteins must be solubilised first and then are loaded onto the 1D-gel. During the 1D-gel separation any remaining lysis buffer derived detergents are efficiently removed from the samples. This is crucial because detergents (e.g. SDS) ionize well and are in huge excess relative to the proteins. Protein bands in the bottom part of the 1D-gel are cut out and tryptic in-gel digestion of proteins is carried out. Eluted peptides from one single band are separated by nano-flow liquid-chromatography (nano-LC) and then identified by tandem mass spectrometric (MSMS) analysis.

3.3.1.1 Reagents and solutions

1,4-Dithio-D,L threitol (DTT), high purity	Gerbu
3-[(3-cholamidopropyl)dimethylammonio]-1-propanesulfonate (CHAPS)	Gerbu
Acidic acid	J.T. Baker
Acryl Amide (AA)	Gerbu
Ammonium persulfate (APS)	Sigma
Deoxycholate	Sigma
Formaldehyde	Merck
Methanol	Sigma
N,N,N',N'-Tetramethylethylendiamine (TEMED)	Sigma
Protease inhibitors 100X	Roche
Silver nitrate	Sigma
Sodium carbonate	Merck
Sodium dodecyl sulfate (SDS)	Gerbu
Sodium thiosulfate	Merck
Thiourea	Sigma
Tris	Gerbu
Urea	Gerbu

	Stock	Final concentration	V_E = 20 ml
Lysis Buffer	Powder	8 M Urea	
	Powder	2 M Thiourea	
	Powder	4% CHAPS	
	Powder	65 mM DTT	
	10% deoxycholate	1% deoxycholate	Fresh
	Protease inhibitors 100X	Protease inhibitors 1X	Fresh

3.3.1.2 Procedure

Mitochondrial protein solubilisation

The final mitochondrial pellet, obtained after the differential centrifugation procedure, was resuspended in a volume of lysis buffer appropriate for the size of the pellet. In general it is desirable to keep the volume low, not diluting the mitochondria too much. Since urea is part of the lysis buffer it was important that all further steps were carried out at room temperature, because at lower temperature there is the risk that proteins might irreversible precipitate. One should also take care not to heat the lysis buffer because carbamylation might occur to amino acid groups of proteins. Once the mitochondrial pellet was resuspended in lysis buffer, the suspension was incubated at room temperature for at least 30 minutes under constant shaking. Following this incubation samples were centrifuged for 1 hour at 25.000 g at room temperature. The supernatant (i.e. mitochondrial protein lysate) was subjected to protein concentration determination using the Bradford method.

1D Shotgun Gel

1.5mm (amount for 2 gels)	Bottom Gel (12%)	Stacking Gel (6%)
H_2O	3 ml	13.2 ml
30% AA/Bis-AA	3 ml	2.4 ml
2 M Tris pH 8.8	1.5 ml	-
1 M Tris pH 6.8	-	2.3 ml
20% SDS	37 µl	90 µl
TEMED	2.8 µl	18 µl
10% APS	34 µl	90 µl

1D shotgun gels were poured the day before the run to ensure proper polymerization. On day of use gels were pre-equilibrated with 80 Volts for 10 minutes. Samples were diluted to 100-150 µg and mixed with Laemmli buffer, heated for 5 minutes at 95°C

and then loaded on to the gel. Stacking gels were running at constant 80 V for about 2 hours. When samples reached the bottom gel the voltage was increased to constant 100 V for another 15-30 min.

Silver nitrate staining

Fix	50% methanol/10% acetic acid
Wash	50% methanol
Sensitize	0.02% $Na_2S_2O_3$*$5H_2O$
Stain	0.1% $AgNO_3$
Develop	3%Na_2CO_3/0,5%HCHO
Stop/Store	1% acetic acid
Rinse/Wash	ddH_2O

Immediately after electrophoresis was finished gels were fixed for at least 1 hour (typically over night) in 50% methanol/10% acetic acid at 4°C. To get rid off the acetic acid gels were washed with 50% methanol for 10 minutes, followed by another two wash steps with ddH_2O for 5 minutes each. Next gels were sensitized for 30 seconds with 0.02% $Na_2S_2O_3$*$5H_2O$, then rinsed two times with ddH_2O, before they were stained with silver nitrate. Gels were stained in a 0.1% $AgNO_3$ solution for 2 x 5 minutes. After staining gels were rinsed again two times with ddH_2O. With 3% Na_2CO_3/0.5% HCHO gels were developed. This reaction was stopped with 1% acetic acid. Finally gels were washed two times with ddH_2O and scanned. If gels were not immediately used they were stored in 1% acetic acid at 4°C.

3.3.2 Mass spectrometry analysis

In Mass spectrometry (MS) molecules are analysed by measuring the masses of ions. Therefore ions are generated from either inorganic or organic compounds, which are then separated by their mass-to-charge ratio (m/z). Ions are detected qualitatively and quantitatively by their respective m/z and abundance.

MS consists in principle of 3 components: an ion source, an analyser and an ion detector. The sample is either directly introduced into the ion source or into a chromatographic system that is placed upstream of the ion source. Electrospray ionization (ESI) and matrix-assisted laser desorption/ionization (MALDI) are the two major ion sources used. In our studies we used ESI. Here the sample is dissolved in a polar, volatile solvent such as acetonitrile and subsequently injected into a metal

capillary. At the end of the capillary a high voltage is applied causing the dispersion of the sample into an aerosol of highly charged droplets. Due to the evaporation of the solvent, the droplets become smaller and charge density increases. Analyte ions desorbing from the droplet surface produce desolvated ions, which then enter the mass spectrometer. There are three main types of mass spectrometers: Quadrupole MS, Time Of Flight (TOF) MS and Quadrupole ion traps. These mass spectrometers differ in how they determine the mass-to-charge ratio. Furthermore, it is possible to combine these analysers, referred to as tandem mass spectrometry (MS/MS). In our study we used tandem MS/MS to analyse our biological samples. In the detector the current of the ions is monitored, amplified and transmitted to the data system. There the mass spectra are recorded, and m/z values are plotted against their intensities.

3.3.2.1 Reagents and solutions

2,2,2-trifluoroethanol (TFE)	Sigma
Acetic acid (HAc)	J.T. Baker
Acetic acid (HAc) 100% Suprapur	VWR International
Acetonitrile (ACN)	Fluka
Acetonitrile (ACN) HPLC grade	VWR International
Ammonium Bicarbonate	Fluka
Dithiothreitol (DTT)	Gerbu
Formic Acid (FA)	Merck
Formic Acid (FA) 98-100% Suprapur	VWR International
Iodoacetamide (IAA)	Sigma
Methanol	Sigma
Potassium hexacyanoferrate ($K_3Fe(CN)_6$)	Sigma
Sodium thiosulfate ($Na_2S_2O_3$)	Merck
Trypsin	Promega

	Final concentration
Destaining solution	15 mM $K_3Fe(CN)_6$ 50 mM $Na_2S_2O_3$ in ddH_2O
Wash solution	50% Methanol 10% HAc in ddH_2O
pH neutralizing solution	50 mM NH_4HCO_3 in ddH_2O
Reducing solution	10mM DTT in 50 mM NH_4HCO_3
Alkylation solution	10.2 mg IAA/ml in 50 mM NH_4HCO_3
Digestion buffer	15 ng/µl Trypsin in 50mM NH_4HCO_3
Elution buffer	2% Formic Acid 50% ACN 48% ddH_2O

3.3.2.2 Procedure

In-gel tryptic digestion

Stained gels were put on the Gel DOC 1000 White Light Source and each lane was cut into 5-10 gel slices. Gel pieces were either immediately processed or they were stored at 4°C in 1.5 ml Eppendorf tubes filled with 1% acetic acid. Tryptic digestion was performed under a clean keratin-free laminar flow. Gel-pieces were destained with destaining solution under constant shaking followed by an intensive wash step with 50% methanol 10% acetic acid over night. The pH of gel-pieces was neutralized the next day with 50 mM NH_4HCO_3 and subsequently gel-pieces were dried with acetonitrile (ACN). Next, proteins were reduced with 10 mM DTT in 50 mM NH_4HCO_3 at 56°C for 60 minutes and alkylated with 50 mM IAA in 50 mM NH_4HCO_3 in the dark for 20 minutes. Between these two steps gel pieces were dried with ACN. After alkylation the pH of gel-pieces was neutralized with 50 mM NH_4HCO_3 and then dried with ACN. Dry gel-pieces were rehydrated in 20 µl digestion buf fer for 30 minutes on ice. Gel-pieces were covered with 25 mM NH_4HCO_3 and incubated at 37°C over night. The next day tubes were centrifuged and the supernatant was transferred to a 0.5 ml clear view snap cap tube. Gel-pieces were covered with 5% formic acid 50% ACN and ultrasonicated at 160 W for 10 minutes (VWR Ultrasonic Cleaner). Again tubes were centrifuged and the supernatant was transferred to a fresh 0.5 ml clear view snap cap

tube. This elution procedure was repeated another time. Finally the peptide solution was concentrated in a vacuum centrifuge to a total volume of about 20 μl.

Protein identification and interpretation (Mass spectrometry)

For protein identification we used an UltiMate Plus nano HPLC system (Dionex, Amsterdam, The Netherlands) coupled to the Velos Ion-Trap mass spectrometer (Thermo Fisher Scientific, Bremen, Germany).

Tryptic digests from each lane of the 1D-Gel were loaded on a C18 trap column with 0.1% TFE. Separation on a nano C18 column was performed by applying an acetonitrile gradient composed by mixing the following mobile phases: A: 95% water, 5% ACN, 0.1% FA; B: 70% water, 15% ACN, 15% MeOH, 0.1% FA, C: 10% TFE, 80% ACN, 10% MeOH, 0.08% FA. During the first 10 min of the separation the amount of B was increased from 5% B to 15% B. At 8 minutes after the injection the trap column is switched in-line with the separation column. From 10 to 75 minutes the amount of B was increased to 100%. Subsequently, the C was increased from 0% to 100% over the next 20 minutes (from 75 to 95 minutes), and the amount of B reduced to 0%. Next, the column was washed for 10 minutes with 100% C, and then equilibrated with 95% A and 5% B for 15 minutes.

Peptides eluted from the nano separation column were detected with both UV detection at 214 nm and MS/MS detection by nano ESI in positive mode. For the MS detection of peptides, one MS full scan was followed by 10 MS/MS scans of the ten most intensive precursor signals. Database searching of the MS data obtained was performed with Mascot 2.3.02 (Matrix Science, London, UK). Briefly, an MS/MS ions search was performed with carbamidomethylation on cysteine as a fixed modification, and oxidation on methionine, phosphorylation on serine, threonine, or tyrosine as variable modifications. Monoisotopic masses were searched within unrestricted protein masses for tryptic peptides. The peptide mass tolerance was ±0.8 Da and the fragment mass tolerance ±0.5 Da. The maximal number of missed cleavages was set to 2. The minimum ion score for peptide identifications in Mascot was set to 20. Scaffold 3.0 (Proteome Software Inc., Portland, OR, USA; www.proteomesoftware.com) was used to improve visualization, sensitivity, and validity of results. The software package verifies peptide identifications assigned by Mascot using the X!Tandem database searching program. Scaffold then

probabilistically validates these peptide identifications using PeptideProphet, and derives corresponding protein probabilities using ProteinProphet. We further processed all our mass data with the Scaffold software tool to validate MS/MS based peptide and protein identifications. Only proteins containing at least 2 identified peptides with an identification probability >95% were accepted. Proteins that could not unambiguously be identified by automated MS/MS analysis alone – e.g. because they contained similar peptides – were manually verified. With these stringent data filtering criteria we wanted to reach a false discovery rate (FDR) of a maximum of 2% on the protein level. The modified protein list was interpreted with the David bioinformatics database and further compared with the MitoCarta database (www.broadinstitute.org/pubs/MitoCarta) and the GO annotation database (www.geneontology.org) to exclude all non-mitochondrial proteins from the list and obtain a mitochondrial protein list.

Since analysis of differentially expressed proteins may not always lead to the generation of a list of proteins with a unifying and clear biological theme, we analysed our proteomic dataset by gene set enrichment analysis (GSEA; www.broadinstitute.org/gsea)[113]. To perform the GSEA analysis we created a list encompassing the number of unique peptides (L1) and a list encompassing the number of unique spectra (L2) obtained from mass spectrometry. Using GSEA the lists were searched against a priori defined gene sets. We compared our lists with a cytogenetic set (C1), a functional set (C2) and GO category set (C5). The purpose of GSEA is to define if members of a certain gene set are primarily found at the top or the bottom of a ranked list or if they are randomly distributed throughout the list. The so-called enrichment score (ES) is the measure whether a gene set is overrepresented at the top or the bottom of the ranked list. The statistical significance (nominal p value) of the ES is estimated by an empirical phenotype-based permutation test procedure. For our analysis we used a number of 1000 permutations. Gene sets larger than 500 and gene sets smaller than 5 genes were excluded from our analysis.

3.4 Western Blot

In this technique proteins are separated according to their mass by SDS-PAGE (sodium dodecyl sulphate-polyacrylamide gel electrophoresis), and subsequently transferred onto a support membrane such as polyvinylidene fluoride (PVDF). There proteins stick to the surface due to hydrophobic interactions. With the use of specific antibodies protein bands on the membrane can be visualised. The PVDF membrane is incubated with the primary antibody which is specific for a certain epitope. A secondary antibody recognizes and binds the Fc-part of the primary antibody, and is conjugated to an enzyme (typically horse radish peroxidise, HRP). Addition of an HRP-substrate visualizes the protein bands, which are detected by a chemiluminescence scanners.

3.4.1 Reagents and solutions

1,4-Dithio-D,L threitol, high purity (DTT)	Gerbu
2-Mercapto Ethanol (β-ME)	Sigma
30% Acrylamide/Bis Solution 29:1 (3,3% C)	Bio-Rad
Ammonium persulfate (APS)	Sigma
Bovine Serum Albumin, fatty acid free (BSA)	PAA
Bromphenolblue (BPB)	Sigma
Glycerol 99.8%	Fluka
Glycine	Gerbu
Methanol	Sigma
N,N,N',N'-Tetramethylethylendiamine (TEMED)	Sigma
PageRuler Plus Prestained Protein Ladder	Fermentas
PhosStop Phosphatase Inhibitor Cocktail tablets	Roche
Protease Inhibitors 100X	GE Healthcare
Sodium dodecyl sulfate (SDS)	Gerbu
SuperSignal West Femto Kit	Thermo Scientific
SuperSignal West Pico Kit	Thermo Scientific
Tris	Gerbu
Tween 20	Sigma

	Stock	Final concentration	V_E = 9 ml
4X Laemmli buffer*	1 M	60 mM Tris pH 6,8	2.4 ml
		2% SDS	0.8 g
		10% Glycerol	4 ml
	0.1%	0.0012% BPB	0.8 ml
	4 M	100 mM DTT	add prior to use
	*store 1 ml aliquots at -20°C		

	Stock	Final concentration	V_E=100 ml
10X Running buffer		0.25 M Tris	30.3 g
		2 M Glycin	150 g
	20% SDS	1% SDS	50 ml

	Stock	Final concentration	V_E= 1 l
10X Transfer buffer		250 mM Tris	30.3g
		1.92M Glycine	144.1g
	Add 10% methanol to 1X solution and store at 4°C		

	Stock	Final concentration	V_E= 1 l
10x TBS pH 7.5		Tris	12.1g
		NaCl	87.6g
	Add 0.2% Tween 20 to 1X solution		

	Stock	Final concentration	V_E = 100 ml
Stripping buffer	20% SDS	2% SDS	10 ml
		100 mM βME	0.7 ml
		65.2 mM Tris pH 6,8	6.25 ml

Primary Antibody	**3% BSA in TBS-T**	
β-Actin	1:10000	Sigma
Calnexin	1:5000	Sigma
Complex V	1:1000	mito science
Histone H3	1:2000	Cell signaling
LAMP2	1:2000	abcam

Secondary Antibody	**3% BSA in TBS-T**
Anti-mouse	1:4000
Anti-rabbit	1:4000

3.4.2 Procedure

SDS-Gel

Gels were poured in the order indicated in the table below. If gels were not used immediately they were wrapped in a plastic foil together with a piece of wet paper and stored at 4°C for a few days.

1 mm Bottom Gel (2 Gels, 10 ml)		
	8%	12%
1. ddH2O	5,3 ml	4 ml
2. 30% AA/BisAA	2,7 ml	4 ml
3. 2 M Tris pH 8,8	1,9 ml	1,9 ml
4. 20% SDS	50 µl	50 µl
5. TEMED	10 µl	10 µl
6. 10% APS	100 µl	100 µl

1 mm Stacking Gel (2 Gels, 5 ml)	
	6%
1. ddH2O	3,3 ml
2. 30% AA/BisAA	1,0 ml
3. 2 M Tris pH 6,8	625 µl
4. 20% SDS	25 µl
5. TEMED	5 µl
6. 10% APS	50 µl

SDS-PAGE

Protein samples in Laemmli buffer were boiled for 5 minutes at 95°C and placed on ice until they were loaded onto the gel. Protein ladder and samples were loaded into the wells and gels were running at constant 60 V until samples reached the border of bottom and stacking gel, continuing with constant 120 V until the migration front nearly reached the end of the gel.

Wet protein transfer

For the protein transfer we used PVDF membranes. PVDF membranes were activated by soaking them in 100% methanol for 30 seconds, washed for 2 minutes in distilled water, and finally equilibrated in transfer buffer for at least 3 minutes. Protein transfer was then carried out at 4°C at a constant voltage of 20 Volts for 10 minutes, 50 Volts for 10 minutes and 100 Volts for one hour.

Immunodetection

Following the protein transfer membranes were blocked either in 5% BSA or 5% milk solution in TBS/Tween 20 (TBS-T) for 1 hour at room temperature. Next, blots were incubated with primary antibody solution over night at 4°C. The next day primary antibody solution was taken off and stored at -20°C for further usage. The membrane was washed 3 times with TBS-T for 10 minutes at room temperature and then incubated with secondary antibody solution for 1 hour at room temperature. Again

the membrane was washed 3 times with TBS-T as mentioned above. For chemiluminescence-immunodetection the membrane was incubated for approximately 1 minute with the SuperSignal West Femto and Pico Kits (Pierce). Chemiluminescence signals were detected using a Bio-Rad Imager (ChemiDoc XRS).

3.5 Quantitative real time PCR (q-PCR)

Primarily this technique is used to measure mRNA levels of respective target genes. In our case we also used it to measure the amount of mitochondrial DNA (mtDNA). If mRNA levels are to be detected then the mRNA is transcribed first into cDNA. The DNA is then amplified with a PCR reaction, only that the PCR products are detected in real time. There are several methods available to detect PCR products. We use the fluorogenic dye SYBR Green, which emits a strong fluorescent signal when it binds to dsDNA.

3.5.1 Reagents and solutions

Ethylenediaminetetraacetic acid (EDTA)	Sigma
High capacity cDNA reverse transcription Kit	Applied Biosystems
iTaq SYBR Green Supermix with ROX	Bio Rad
Sodium Chloride (NaCl)	Sigma
PBS 1X	Sigma
peqGOLD Total RNA Kit	PEQLAB
Proteinase K	Roche
Sodium dodecyl sulfate (SDS)	Gerbu
Tris	Gerbu

3.5.2 Procedure

RNA Isolation

Total RNA was isolated using the "peqGOLD Total RNA Kit" according to the manufacturer's instructions. Briefly, cells were washed with 1X PBS and then 400 µl of RNA Lysis Buffer T was equally added to the cell layer. Cell lysates were either snap frozen in liquid nitrogen and stored at -80°C or immediately processed. For RNA isolation the lysate was first loaded to a DNA Removing Column, which was placed in a 2 ml collection tube, and centrifuged at 12.000 g for 1 minute at room temperature. The flow through was collected and mixed with an equal volume of 70% ethanol. The sample was loaded on a PerfectBind RNA Column placed in a 2 ml collection tube, and centrifuged with 10.000 g for 1 minute at room temperature. Flow through was discarded and the column was loaded with 500 µl RNA wash buffer 1 and centrifuged with 10.000 g for 15 seconds at room temperature. Flow through was again discarded

and the column was loaded with RNA wash buffer 2 and centrifuged as mentioned in the wash step before. This wash step was repeated another time. Then the empty column was centrifuged at 10.000 g for 2 minutes at room temperature for drying. RNA was eluted with 50-100 µl sterile RNase-free ddH_2O by centrifugation at 5.000 g for 1 minute at room temperature and subsequently stored at -80°C.

DNA Isolation

	Stock	**Final concentration**	**V_E = 25 ml**
DNA Isolation Buffer	100 mM Tris HCl pH 8.5	10 mM Tris HCl pH 8.5	2.5 ml
	0.5 M EDTA	5 mM EDTA	0.25 ml
	10% SDS	0,2% SDS	0.5 ml
	5 M NaCl	200 mM NaCl	1 ml
	20 mg/ml Proteinase K	0.1 mg/ml Proteinase K	0.125 ml
	ddH_2O		23.125 ml

Cells were washed with 1X PBS, then DNA isolation buffer was added directly to the cell monolayer (300 µl/24-well) and incubated at 37°C for at least 2-3 hours or over night. Lysates were transferred to Eppendorf tubes and incubated at 99°C for 10 minutes to heat inactivate the Proteinase K. An equal volume of isopropanol was added to the lysate and incubated for 10-20 minutes at room temperature under constant shaking to precipitate the DNA. To pellet the precipitate, samples were centrifuged at 10.000 rpm for 10 minutes at 4°C. The Supernatant was discarded, the pellet air dried and then finally resuspended in an appropriate volume of TE (10 mM Tris HCl, 0.1 mM EDTA; pH 7.5).

cDNA Synthesis

For reverse transcription of RNA samples, we used the "high capacity cDNA reverse transcription kit" from Applied Biosystems. Synthesis of cDNA was carried out according to the manufacture's instructions. In brief, we 10 µl of total RNA (i.e. 100 ng RNA) were mixed with 10 µl of the reverse transcription master mix.

Component	**Volume/reaction (µl)**
10X RT Buffer	2.0
25X dNTP Mix (100 mM)	0.8
10X RT Random Primers	2.0
MultiScribe Reverse Transcriptase	1.0
Nuclease-free H2O	4.2
TOTAL	**10.0**

Tubes were closed and briefly centrifuged to get rid of any air bubbles, and placed on ice until being loaded into the thermal cycler (Eppendorf Mastercycler pro S).
For reverse transcription the following cycling program was used:

	Step 1	**Step 2**	**Step 3**	**Step 4**
Temperature (°C)	25	37	85	4
Time	10min	120min	5sec	∞

q-PCR

q-PCR was performed using the iTaq SYBR Green Supermix with the C1000 Thermal Cycler CFX96TM Real Time System (BioRad) and the following settings:

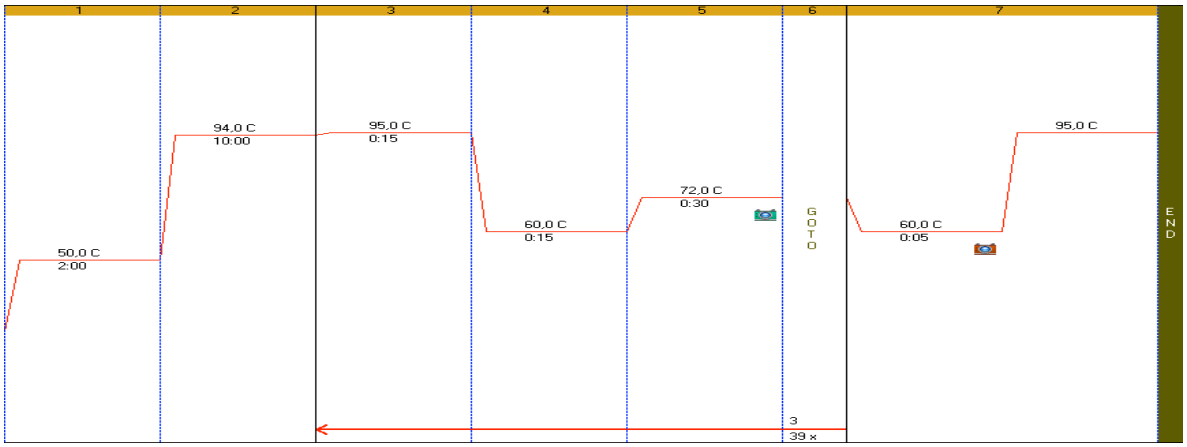

Post-amplification melting curve analysis was performed to make sure that no unspecific products were amplified. None-template controls (NTC) were included to ensure that no primer dimers were amplified. Resulting data were evaluated using the comparative C_t method (also known as delta delta C_t method). Threshold cycles (C_t-values) of all samples were normalized to the housekeeping gene Rplp0/Arp to obtain ΔC_t values (= C_t gene of interest - C_t Arp). To compare the effect of treatment with untreated control $\Delta\Delta C_t$ values (= ΔC_t treatment - ΔC_t control) were calculated first, followed by the calculation of $2^{-\Delta\Delta Ct}$ values to obtain fold expression levels. For mtDNA/gDNA ratio experiments gNDUFV1 was used as the endogenous housekeeper for normalization. Primers used are shown below.

Gene symbol	Alias		Sequence (5'-3')
Rplp0	Arp	forward	GCCAATAAGGTGCCAGCTGCTG
		reverse	GAGGTCTTCTCGGGTCCTAG
Gli1		forward	AGTGCCATGCCGCAGCAG
		reverse	CATCTCCACGCCGCTGTC
Mfn1		forward	CAACCAACTGCTTCCTGAGTG
		reverse	CCAGCTGATTAACAGTCTTCACAC
Mfn2		forward	TATAAGAACGAGCTGCACCGC
		reverse	GTCTGCAGTGAACTGGCAATG
Fis1		forward	GCAACTACCGGCTCAAGGAATATG
		reverse	TTATCAATCAGGCGTTCCAGCTC
Dctn2		forward	TTGCACAAGAGCTGGAGGAAC
		reverse	AACTTGTCGTAGGCAGCGTTG
Dnm1l		forward	CTTCTGAGCTATGCGGTGGTG
		reverse	TCCACAGATTCTAAGGTTCGCC
Nrf1		forward	TCGCTCATCCAGGTTGGTAC
		reverse	TGGTTGGCAGTTCTGAAGCATC
Tfam	mtTFA	forward	GCCTGGGGTCTTGTCTGTAT
		reverse	TTTGGGTAGCTGTTCTGTGG
Ndufv1		forward	CTTCCCCACTGGCCTCAAG
		reverse	CCAAAACCCAGTGATCCAGC
ND2	mtND2	forward	AGGGATCCCACTGCACATAG
		reverse	CTCCTCATGCCCCTATGAAA

3.6 Flow cytometry

Flow cytometry is a technique used to analyse certain properties of a cell population. For analysis cells pass the detection unit as single cells. One property of a cell that is measured with flow cytometry is the light scatter, which results of a laser beam crossing a single cell. The light scatter that is detected almost in the line of the laser beam is the so-called forward scatter (FSC) that provides information about the size of the cell. Another property that can be derived from the light scatter is the granularity of a cell. This information is given by the so-called side scatter (SSC), that is the scattered light recorded in a 90° angle to the original laser beam. Additional information about a cell population can be obtained by labelling the cells with fluorescence markers. Depending on the flow cytometer used, different fluorescent markers can be used to analyse a cell population. Typically, monoclonal antibodies targeting specific surface epitopes are used as markers. A secondary antibody, conjugated to a fluorescence signal, conferring them with the fluorescent tag, then recognizes these monoclonal antibodies. Of note, dyes have been developed that specifically stain various cell compartments in an antibody independent manner, thus allowing quantitative measurement of compartment mass and function.

3.6.1 Reagents and solutions

Carbonyl cyanide-*p*-trifluoromethoxyphenylhydrazone (FCCP)	Sigma
DMEM	PAA
Fetal Bovine Serum HI (FBS)	PAA
Mitotracker Green FM	Molecular Probes
Oligomycin	Sigma
PBS 1X	Sigma
Tetramethylrhodamine,ethyl ester **(**TMRE)	Molecular Probes
Trypsin	PAA

3.6.2 Procedure

Mitotracker Green FM and TMRE co-staining

To investigate mitochondrial mass and mitochondrial membrane potential ($\Delta\psi m$) in adipocytes we used two dyes: Mitotracker Green FM and TMRE. The advantage of the

cell-permeant mitochondrion-selective dye Mitotracker Green FM is that it accumulates in mitochondria regardless of their membrane potential and it only becomes fluorescent once it accumulates in the lipid environment of mitochondria. It is therefore an easy to use method to determine mitochondrial mass by FACS analysis. The cell-permeant and cationic dye tetramethylrhodamine ethyl ester (TMRE) is a commonly used dye to determine mitochondrial membrane potential ($\Delta\psi m$). Due to its cationic nature it selectively enters mitochondria depending on their actual membrane potential, i.e. mitochondria with a high membrane potential will accumulate more TMRE than mitochondria with a low membrane potential.

In our experiments we incubated adherent (pre-)adipocytes with serum-free medium containing 100 nM Mitotracker Green FM and 100 nM TMRE for 45 min at 37°C. Afterwards cells were washed once with PBS and then trypsinized. The Trypsin reaction was stopped with an equal amount of DMEM/10% FBS. Next, cells were centrifuged at 200 g for 5 minutes at room temperature. The resulting cell pellet was resuspended in 500 µl prewarmed PBS and analyzed with a FACSCalibur (Becton Dickinson) flow cytometer.

FACS analysis with the FACSCalibur Cytometer

We excluded cellular debris from analysis by using a forward-scatter/side-scatter representation of events. For each sample 30,000 gated events were acquired. Cells were excited with a 488 nm argon laser line. Mitotracker Green FM fluorescence was detected on FL-1 (530 nm) and TMRE fluorescence was detected on FL-2 (585 nm). Data analysis was performed using the FlowJo 7.6.4 software.

A number of events/FL-1 histogram was created, reflecting Mitotracker Green FM fluorescence intensity representing mitochondrial mass. The mean value of the sum of FL-1 intensities was calculated and compared between SAG-treated and untreated control samples. Mitochondrial membrane potential was evaluated in 2 manners. First, the ratio of cells containing high versus low mitochondrial membrane potential was calculated as an accepted indicator for the condition of the mitochondria in the cells. Second, an events/FL-2 histogram was created. Finally, FL-2/FL-1 ratios, representing TMRE/Mitotracker Green FM ratios, were calculated.

3.7. Confocal microscopy

A strong light source (usually laser based) is used as an excitation wavelength. In sharp contrast to standard fluorescence microscopy only emitted light in focus is detected. This is achieved by a pinhole placed in front of the detector, which will pass light only coming from a specific plane. With this technique it is possible to get crisp fluorescent pictures, and analyse the localization of detected signals in high resolution. In addition, confocal microscopy enables to generate a 3-dimensional Z-stack image of scanned samples.

3.7.1 Reagents and solutions

DMEM	PAA
Fetal Bovine Serum HI (FBS)	PAA
Hoechst 33342	Molecular Probes
Mitotracker Green FM	Molecular Probes
PBS 1X	Sigma
Tetramethylrhodamine ethyl ester (TMRE)	Molecular Probes
Trypsin	PAA

3.7.2 Procedure

Live imaging with Mitotracker Green FM and TMRE

Since we did not obtain satisfying results with fixed adipocytes and Mitotracker Red CMXRos, we decided to use Mitotracker Green FM and perform live cell imaging to investigate mitochondrial distribution in mature adipocytes. Additionally, we used the mitochondrion selective dye tetramethylrhodamine ethyl ester (TMRE) together with Mitotracker Green FM to investigate changes in mitochondrial membrane potential since the accumulation of TMRE is driven by the membrane potential. We cultivated the adipocytes in glass bottom culture dishes (MatTek Corporation). After the respective treatment adipocytes were incubated with DMEM containing 100 nM Mitotracker Green FM and 20 nM TMRE for 40 min at 37°C. Subsequently adipocytes were incubated with DMEM containing 5 μg/ml Hoechst and 20 nM TMRE for 10 min at 37°C. For image acquisition adipocytes were maintained in 25 mM HEPES/DMEM

base (without Phenolred), since our confocal microscopes are not equipped with a temperature-controlled chamber supplemented with 20 nM TMRE.

Image acquisition

Images were obtained with a LSM 700 (Zeiss) laser scanning confocal microscope using a 63X oil immersion objective. Pinhole size was adjusted to gain about 1.1 µm thick sections. Image processing was done using the Zen software package (Zeiss, 2009).

3.8. Transmission electron microscopy (TEM)

Transmission electron microscopes (TEM) are able to magnify biological specimen significantly higher than light microscopes. This is due to the emission source used. The maximum resolution that is obtained (2nm are a common resolution) is determined by the wavelength of the emission source, electrons having a substantially smaller wavelength than photons. In a vacuum system electron emission is produced by an electron gun at the top of the microscope. Electron lenses are used to focus the electron beam. The specimen is in part transparent to electrons and in part scatters them out of the beam, constituting the electron microscope picture which can be recorded photographically.

3.8.1 Reagents and solutions

0.2M Sodium-Cacodylate buffer (CaCO)	Fluka
1,2-propylenoxide	Merck
2-Dodecenylsuccinic acid anhydride (DDSA)	Serva
Epon 812	Serva
Formaldehyde	Merck
Glutaraldehyde (GA)	Merck
Glycidyl ether	Serva
Methanol	Fluka
Methylnadic anhydride (MNA)	Serva
Osmium tetroxide (OsO_4)	Agar
Paraformaldehyde (PFA)	Merck
Pb(II)nitrate Reynolds solution	Merck
Potassiumhexacyanoferrate	Merck
Uranylacetate	Agar

Karnovsky stock solution	**V_E=50ml**
PFA	2.0 g in 25ml ddH_2O
1 M Sodium hydroxide	2-4 drops
50% GA	5 ml
0.2 M cacodylate buffer pH 7.4	20 ml

3.8.2 Procedure

Following the respective treatment (24 hours or 48 hours SAG/vehicle control), media was removed and cells were fixed for 30 minutes at room temperature in Karnovsky stock solution. The solution was poured off and cells were immediately scraped off and transferred to Eppendorf tubes and further fixed at room temperature for 60 minutes with Karnovsky solution. Fixed cells were centrifuged for 1 minute at 2000 rpm. Cells were shortly rinsed and resuspended in CaCO buffer and incubated for 30 minutes at room temperature. This step was repeated one more time. For EPON embedding the loose pellets were stored in CaCO buffer until further processing. Part of the samples were transferred to fresh Eppendorf tubes to prepare agarose pellets.

Agarose embedding procedure

The pellet was rinsed with PBS and then centrifuged for 1 minute at 2000 rpm at room temperature. Next the pellet was heated to 60°C. At the same time 10% agarose was also heated to 60°C and mixed with the pellet and immediately centrifuged for 2 minutes at 2000 rpm. Right after the centrifugation the samples were cooled on ice for 3 hours. Chilled pellets were stored in CaCO buffer.

EPON embedding procedure

Loose cell pellets were centrifuged after each step for 1 minute at 2000 rpm and all steps were carried out at room temperature unless stated otherwise. First, cell pellets were incubated 2 times for 30 minutes at room temperature in 0.1 M CaCO buffer. This was followed by a 3 hour incubation step in 1% OsO_4/potassiumhexacyanoferrate. Pellets were washed twice with ddH_2O for 5 minutes and were then dehydrated with increasing levels of alcohol (70%-80%-96%-100%) each 2 times for 10 minutes. Dehydrated pellets were incubated twice for 10 minutes in 1,2-propylenoxide, followed by an incubation of 60 minutes in EPON 812/1,2-propylenoxide (1:1 resin mixture). Finally, pellets were incubated over night in pure EPON 812. The next day samples were mounted with fresh resin in silicon shapes and subjected to final polymerisation at 60°C for the next 2-3 days.

Cutting and microscopy

Blocks were cut in ultrathin sections (80 nm) using a Leica EM UC7 microtom. Sections were placed on a cupper mesh and dried. Subsequently slices were treated with 0.05% uranylacetate/methanol for 4 min, followed by a 3 minutes of treatment with Pb(II)nitrate Reynolds solution. Image acquisition was done with a JEOL 1010 TEM.

3.9. Statistical Analysis

Data are presented as mean ± standard error of the mean (SEM). To analyse differences between groups the unpaired student's t-test was applied. P values <0.05 were considered to be statistically significant.

4. RESULTS

Our main focus in the investigation of putative changes in adipocyte mitochondria treated with SAG was the 1D-GeLC/MSMS analysis. Here we were interested if a difference in the mitochondrial proteome of SAG treated 3T3-L1 adipocytes could be observed. Furthermore we applied several techniques to investigate changes in certain mitochondrial properties. We used for instance FACS analysis and confocal microscopy to determine changes in mitochondrial volume and mitochondrial membrane potential (Δψm). qPCR was performed to examine changes in mtDNA content and RNA expression of particular genes important for mitochondrial fusion and fission. Finally, to look for differences in mitochondrial shape and ultra structure electron microscopy was applied.

4.1 Mitochondrial Proteomics

The mitochondrial proteome of SAG treated 3T3-L1 mature adipocytes was analysed as depicted in Figure 8.

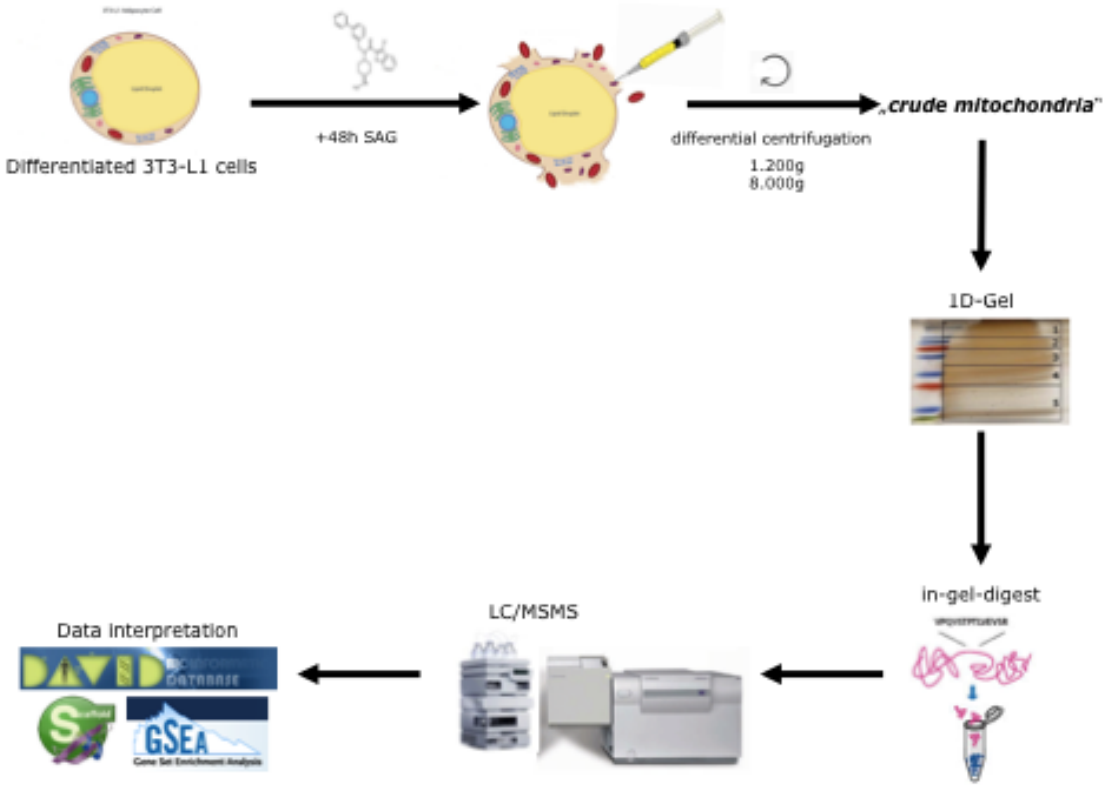

Figure 8 Schematic presentation of the proteomics approach Mature 3T3-L1 adipocytes were stimulated for 48 hours with SAG. A crude mitochondrial fraction was isolated by differential centrifugation and further subjected to 1D-Gels. Every sample was divided into 5 lanes and in-gel digested, analysed by LC/MSMS. Results were interpreted with Scaffold, David bioinformatics database and GSEA.

Differentiated 3T3-L1 cells of day 5 were starved for 18 hours and subjected to 48 hours of SAG treatment. Mitochondrial proteins were isolated as described in the Materials and Methods section. 1D-Gel electrophoresis was performed and separated proteins were in-gel digested by the protease Trypsin.

Peptides were separated by nanoflow LC and identified by MSMS fragmentation analysis. Spectral counting was performed to determine the relative protein abundance in treated and untreated samples. We used the Scaffold Viewer to modify the protein list and interpreted the list with David, a free bioinformatics database. Furthermore we performed a gene set enrichment analysis (GSEA) with the obtained protein list.

4.1.1 Differential centrifugation yielded only a crude mitochondrial fraction

To compare mitochondrial proteomes between treated and untreated adipocytes we did not intend to obtain highly pure mitochondria. Rather our goal was to isolate crude mitochondria and perform a GO-term post hoc exclusion analysis.

As shown in Figure 9 our isolated crude mitochondrial fraction was contaminated with some endoplasmatic reticulum (ER) and lysosomes but not with components of cytosol or nucleus. Nevertheless, mitochondrial proteins were enriched in the mitochondrial fraction.

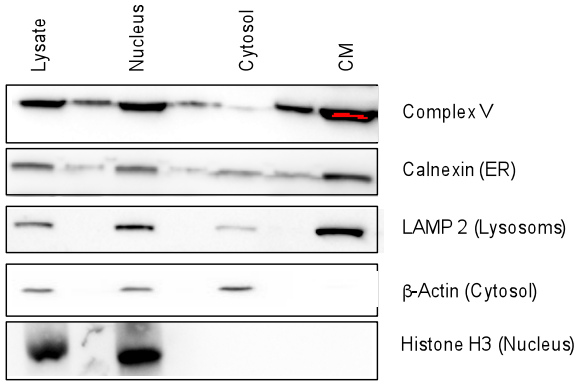

Figure 9 Crude mitochondrial (CM) isolation: Western blots showing the enrichment of certain cell compartments of different isolation aliquots. It can be clearly pointed out that this isolation procedure results in crude mitochondria contaminated with other organelles such as lysosomes and endoplasmatic reticulum.

4.1.2 Depth and coverage of the 3T3-L1 mitochondrial proteome

The 1D-GeLC/MSMS approach was performed in quadruplicates. Only proteins with an identification probability >95% and at least 2 unique peptides were retained in the protein list. After these stringent data filtering criteria were applied we obtained a final protein list with a total of 408 proteins with a false discovery rate (FDR) of 0.1%

at protein level and 0.8% at the unique peptide level. To assess the mitochondrial purity of our samples we compared our protein list with public databases: the MitoCarta database (www.broadinstitute.org/pubs/MitoCarta) and the GO annotation database (www.geneontology.org). Overlaps of our protein list with these two databases are depicted as Venn-diagrams in Figure 10 A & B. From our 408 proteins 244 proteins are assigned to mitochondria according to the MitoCarta database and 276 proteins according to the GO annotation database. This corresponded to a purity of ranging from 59.8% to 67.6% in our isolation. Main contaminations comprised ER proteins (as shown by Western blot Fig. 9) but also proteins from the nucleus, Golgi apparatus and the plasma membrane (Figure 10 C). After comparison with these two databases we generated a mitochondrial protein list encompassing 277 proteins (Table 4-1).

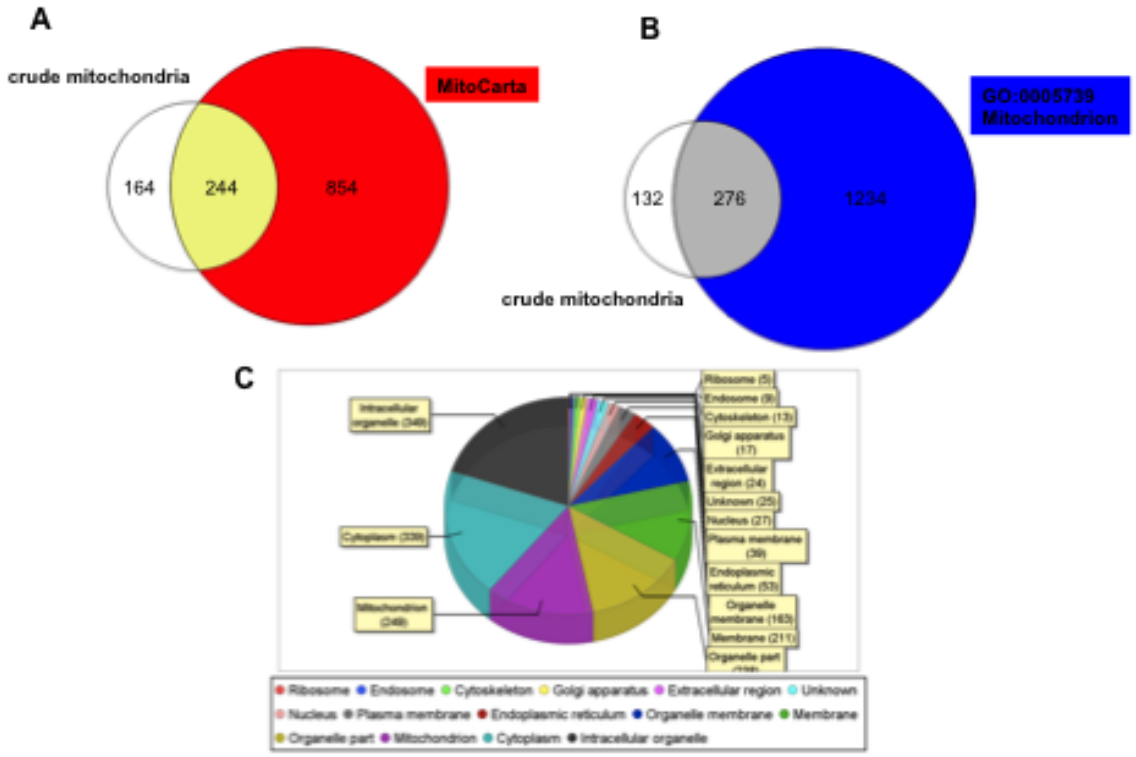

Figure 10 Venn diagrams showing the number of shared proteins between our crude mitochondrial fractions and the (a) MitoCarta dataset (1098 genes/proteins) and the (b) GO annotation database – GO:0005739 mitochondrion (1512 genes/proteins). (c) Pie chart showing the distribution of identified proteins according to Gene ontology terms (GO terms) from the NCBI database

Table 4-1 – Mitochondrial proteins detected

	Protein (277)	Gene name	mol. Mass [kDa]	Max. unique peptides
1	UPF0465 protein C5orf33 homolog	1110020G09Rik	51 kDa	2
2	Uncharacterized protein KIAA0564 homolog	1300010F03Rik	213 kDa	29
3	Protein QIL1	2410015M20Rik	13 kDa	3
4	Uncharacterized protein C18orf19 homolog	4933403F05Rik	32 kDa	2
5	Transmembrane protein C9orf46 homolog	5033414D02Rik	17 kDa	3
6	UPF0765 protein C10orf58 homolog	5730469M10Rik	24 kDa	5
7	Uncharacterized protein C2orf47 homolog, mitochondrial	9430016H08Rik	33 kDa	2
8	Alanyl-tRNA synthetase, mitochondrial	Aars2	107 kDa	2
9	Aspartate aminotransferase, mitochondrial	Abcd3	47 kDa	16
10	3-ketoacyl-CoA thiolase A, peroxisomal	Acaa1A	44 kDa	10
11	3-ketoacyl-CoA thiolase, mitochondrial	Acaa2	42 kDa	18
12	ATP-binding cassette sub-family D member 3	Acad9	75 kDa	2
13	Acyl-CoA dehydrogenase family member 9, mitochondrial	Acadl	69 kDa	8
14	Long-chain specific acyl-CoA dehydrogenase, mitochondrial	Acadm	48 kDa	19
15	Medium-chain specific acyl-CoA dehydrogenase, mitochondrial	Acads	46 kDa	25
16	Acyl-CoA-binding protein	Acadsb	10 kDa	4
17	Short-chain specific acyl-CoA dehydrogenase, mitochondrial	Acadvl	45 kDa	13
18	Acetyl-CoA acetyltransferase, mitochondrial	Acat1	45 kDa	15
19	Acyl-CoA desaturase 1	Aco2	41 kDa	5
20	Short/branched chain specific acyl-CoA dehydrogenase, mitochondrial	Acot13	48 kDa	10
21	Aconitate hydratase, mitochondrial	Acot2	85 kDa	42
22	Acyl-coenzyme A thioesterase 2, mitochondrial	Acot9	50 kDa	5
23	Acyl-coenzyme A thioesterase 9, mitochondrial	Acsf2	51 kDa	2
24	Acyl-CoA synthetase family member 2, mitochondrial	Acsl1	68 kDa	9
25	Hydroxyacid-oxoacid transhydrogenase, mitochondrial	Adhfe1	50 kDa	8
26	ADP/ATP translocase 2	Afg3L2	33 kDa	25
27	AFG3-like protein 2	Aifm1	90 kDa	7
28	Adenylate kinase 2, mitochondrial	Ak2	26 kDa	14
29	GTP:AMP phosphotransferase, mitochondrial	Ak3	25 kDa	9
30	Delta-1-pyrroline-5-carboxylate synthase	Aldh18A1	87 kDa	12
31	Apoptosis-inducing factor 1, mitochondrial	Aldh1L2	67 kDa	18
32	Delta-1-pyrroline-5-carboxylate dehydrogenase	Aldh2	62 kDa	9
33	Probable 10-formyltetrahydrofolate dehydrogenase ALDH1L2	Aldh4A1	102 kDa	3
34	Methylmalonate-semialdehyde dehydrogenase [acylating], mitochondrial	Aldh6A1	58 kDa	26
35	Apolipoprotein O	Apool	24 kDa	3
36	ATPase family AAA domain-containing protein 3	Atad3A	67 kDa	5
37	ATP synthase subunit alpha, mitochondrial	Atp5A1	60 kDa	41
38	ATP synthase subunit beta, mitochondrial	Atp5B	56 kDa	28
39	ATP synthase subunit gamma, mitochondrial	Atp5C1	33 kDa	13
40	ATP synthase subunit delta, mitochondrial	Atp5D	18 kDa	5
41	ATP synthase subunit b, mitochondrial	Atp5F1	29 kDa	12
42	ATP synthase subunit d, mitochondrial	Atp5H	19 kDa	11
43	ATP synthase-coupling factor 6, mitochondrial	Atp5J	12 kDa	2
44	ATP synthase subunit f, mitochondrial	Atp5J2	10 kDa	3
45	ATP synthase subunit e, mitochondrial	Atp5I	8 kDa	6
46	ATP synthase subunit g, mitochondrial	Atp5L	11 kDa	6

47	ATP synthase subunit O, mitochondrial	Atp5O	23 kDa	19
48	ATP synthase protein 8	Atp8	8 kDa	2
49	ATP synthase mitochondrial F1 complex assembly factor 2	Atpaf2	33 kDa	3
50	Branched-chain-amino-acid aminotransferase, mitochondrial	Bcat2	44 kDa	16
51	2-oxoisovalerate dehydrogenase subunit alpha, mitochondrial	Bckdha	50 kDa	12
52	2-oxoisovalerate dehydrogenase subunit beta, mitochondrial	Bckdhb	43 kDa	10
53	Bcl-2-like protein 13	Bcl2L13	47 kDa	7
54	Valacyclovir hydrolase	Bphl	33 kDa	6
55	Brain protein 44	Brp44	14 kDa	5
56	Brain protein 44-like protein	Brp44L	12 kDa	5
57	UPF0598 protein C8orf82 homolog	C030006K11Rik	24 kDa	2
58	Complement component 1 Q subcomponent-binding protein, mitochondrial	C1Qbp	31 kDa	3
59	Carbonic anhydrase 5B, mitochondrial	Car5B	37 kDa	3
60	Catalase	Cat	60 kDa	16
61	Caveolin-1	Cav1	21 kDa	6
62	Carbonyl reductase [NADPH] 2	Cbr2	26 kDa	10
63	Carbonyl reductase family member 4	Cbr4	25 kDa	4
64	Coiled-coil-helix-coiled-coil-helix domain-containing protein 2, mitochondrial	Chchd2	16 kDa	3
65	Coiled-coil-helix-coiled-coil-helix domain-containing protein 3, mitochondrial	Chchd3	26 kDa	17
66	CDGSH iron-sulfur domain-containing protein 1	Cisd1	12 kDa	3
67	Putative ATP-dependent Clp protease proteolytic subunit, mitochondrial	Clpp	30 kDa	5
68	ATP-dependent Clp protease ATP-binding subunit clpX-like, mitochondrial	Clpx	69 kDa	2
69	Clathrin heavy chain 1	Cltc	192 kDa	3
70	Citrate lyase subunit beta-like protein, mitochondrial	Clybl	38 kDa	7
71	Catechol O-methyltransferase domain-containing protein 1	Comtd1	29 kDa	4
72	Ubiquinone biosynthesis protein COQ9, mitochondrial	Coq9	35 kDa	7
73	Cytochrome c oxidase subunit 2	Cox2	26 kDa	6
74	Cytochrome c oxidase subunit 4 isoform 1, mitochondrial	Cox4I1	20 kDa	7
75	Cytochrome c oxidase subunit 5A, mitochondrial	Cox5A	16 kDa	8
76	Cytochrome c oxidase subunit 5B, mitochondrial	Cox5B	14 kDa	3
77	Cytochrome c oxidase subunit 6A1, mitochondrial	Cox6A1	12 kDa	3
78	Cytochrome c oxidase subunit 6B1	Cox6B1	10 kDa	3
79	Cytochrome c oxidase subunit 7A2, mitochondrial	Cox7A2	9 kDa	2
80	Carnitine O-palmitoyltransferase 2, mitochondrial	Cpt2	74 kDa	21
81	Carnitine O-acetyltransferase	Crat	71 kDa	16
82	Cardiolipin synthase	Crls1	33 kDa	2
83	Citrate synthase, mitochondrial	Cs	52 kDa	22
84	Cathepsin B	Ctsb	37 kDa	4
85	Cathepsin D	Ctsd	45 kDa	3
86	Cytochrome b5	Cyb5	15 kDa	7
87	Cytochrome b5 type B	Cyb5B	16 kDa	6
88	NADH-cytochrome b5 reductase 3	Cyb5R3	34 kDa	9
89	Cytochrome c1, heme protein, mitochondrial	Cyc1	35 kDa	9
90	Cytochrome c, somatic	Cycs	12 kDa	11
91	ES1 protein homolog, mitochondrial	D10Jhu81E	28 kDa	8
92	Very long-chain specific acyl-CoA dehydrogenase, mitochondrial	Dbi	71 kDa	33

93	Lipoamide acyltransferase component of branched-chain alpha-keto acid dehydrogenase complex, mitochondrial	Dbt	53 kDa	11
94	3,2-trans-enoyl-CoA isomerase, mitochondrial	Dci	32 kDa	9
95	2,4-dienoyl-CoA reductase, mitochondrial	Decr1	36 kDa	10
96	Dehydrogenase/reductase SDR family member 4	Dhrs4	30 kDa	3
97	Dihydrolipoyllysine-residue acetyltransferase component of pyruvate dehydrogenase complex, mitochondrial	Dlat	68 kDa	10
98	Dihydrolipoyl dehydrogenase, mitochondrial	Dld	54 kDa	22
99	Dihydrolipoyllysine-residue succinyltransferase component of 2-oxoglutarate dehydrogenase complex, mitochondrial	Dlst	49 kDa	7
100	DnaJ homolog subfamily A member 3, mitochondrial	Dnaja3	52 kDa	3
101	Delta(3,5)-Delta(2,4)-dienoyl-CoA isomerase, mitochondrial	Ech1	36 kDa	7
102	Enoyl-CoA hydratase domain-containing protein 2, mitochondrial	Echdc2	32 kDa	4
103	Enoyl-CoA hydratase, mitochondrial	Echs1	31 kDa	15
104	Electron transfer flavoprotein subunit alpha, mitochondrial	Etfa	35 kDa	23
105	Electron transfer flavoprotein subunit beta	Etfb	28 kDa	20
106	Electron transfer flavoprotein-ubiquinone oxidoreductase, mitochondrial	Etfdh	68 kDa	9
107	Protein FAM162A	Fam162A	18 kDa	3
108	Regulator of microtubule dynamics protein 1	Fam82B	35 kDa	3
109	Fatty acid synthase	Fasn	272 kDa	15
110	Farnesyl pyrophosphate synthase	Fdps	41 kDa	2
111	Fumarate hydratase, mitochondrial	Fh1	54 kDa	16
112	Protein NipSnap homolog 2	Gbas	33 kDa	5
113	Glutaryl-CoA dehydrogenase, mitochondrial	Gcdh	49 kDa	2
114	Elongation factor G, mitochondrial	Gfm1	84 kDa	9
115	Growth hormone-inducible transmembrane protein	Ghitm	37 kDa	2
116	Glutaredoxin-related protein 5, mitochondrial	Glrx5	16 kDa	4
117	Glutamate dehydrogenase 1, mitochondrial	Glud1	61 kDa	24
118	Aspartate aminotransferase, mitochondrial	Got2	47 kDa	9
119	Glycerol-3-phosphate dehydrogenase [NAD+], cytoplasmic	Gpd1	38 kDa	3
120	Glycerol-3-phosphate dehydrogenase, mitochondrial	Gpd2	81 kDa	12
121	GrpE protein homolog 1, mitochondrial	Grpel1	24 kDa	13
122	Maleylacetoacetate isomerase	Gstz1	24 kDa	2
123	Estradiol 17-beta-dehydrogenase 8	H2-Ke6	27 kDa	4
124	Hydroxyacyl-coenzyme A dehydrogenase, mitochondrial	Hadh	34 kDa	19
125	Trifunctional enzyme subunit alpha, mitochondrial	Hadha	83 kDa	44
126	Trifunctional enzyme subunit beta, mitochondrial	Hadhb	51 kDa	25
127	Haloacid dehalogenase-like hydrolase domain-containing protein 3	Hdhd3	28 kDa	4
128	Heme-binding protein 1	Hebp1	21 kDa	3
129	3-hydroxyisobutyrate dehydrogenase, mitochondrial	Hibadh	35 kDa	19
130	3-hydroxyisobutyryl-CoA hydrolase, mitochondrial	Hibch	43 kDa	15
131	Histidine triad nucleotide-binding protein 2, mitochondrial	Hint2	17 kDa	3
132	Hexokinase-1	Hk1	108 kDa	3
133	Hexokinase-2	Hk2	103 kDa	34

134	Hydroxymethylglutaryl-CoA lyase, mitochondrial	Hmgcl	34 kDa	2
135	Ribonuclease UK114	Hrsp12	14 kDa	3
136	3-hydroxyacyl-CoA dehydrogenase type-2	Hsd17B10	27 kDa	13
137	Peroxisomal multifunctional enzyme type 2	Hsd17B4	79 kDa	13
138	Hydroxysteroid dehydrogenase-like protein 2	Hsdl2	54 kDa	4
139	Stress-70 protein, mitochondrial	Hspa9	74 kDa	37
140	60 kDa heat shock protein, mitochondrial	Hspd1	61 kDa	48
141	10 kDa heat shock protein, mitochondrial	Hspe1	11 kDa	11
142	Serine protease HTRA2, mitochondrial	Htra2	49 kDa	2
143	Isoleucyl-tRNA synthetase, mitochondrial	Iars2	113 kDa	20
144	Isocitrate dehydrogenase [NADP], mitochondrial	Idh2	51 kDa	16
145	Isocitrate dehydrogenase [NAD] subunit alpha, mitochondrial	Idh3A	40 kDa	21
146	Isocitrate dehydrogenase [NAD] subunit gamma, mitochondrial	Idh3G	?	12
147	Mitochondrial inner membrane protein	Immt	84 kDa	46
148	Isochorismatase domain-containing protein 2A, mitochondrial	Isoc2A	22 kDa	7
149	Isovaleryl-CoA dehydrogenase, mitochondrial	Ivd	46 kDa	13
150	Aldehyde dehydrogenase, mitochondrial	Lap3	57 kDa	20
151	Probable leucyl-tRNA synthetase, mitochondrial	Lars2	101 kDa	3
152	L-lactate dehydrogenase A chain	Ldha	36 kDa	2
153	LETM1 and EF-hand domain-containing protein 1, mitochondrial	Letm1	83 kDa	20
154	Lon protease homolog, mitochondrial	Lonp1	106 kDa	36
155	Lysophospholipid acyltransferase 5	Lrpprc	56 kDa	41
156	Acyl-protein thioesterase 1	Lypla1	25 kDa	2
157	MACRO domain-containing protein 1	Macrod1	35 kDa	3
158	Membrane primary amine oxidase	Maoa	85 kDa	4
159	E3 ubiquitin-protein ligase MARCH5	March5	31 kDa	6
160	Methylcrotonoyl-CoA carboxylase subunit alpha, mitochondrial	Mccc1	79 kDa	12
161	Methylcrotonoyl-CoA carboxylase beta chain, mitochondrial	Mccc2	61 kDa	10
162	Malate dehydrogenase, cytoplasmic	Mdh1	37 kDa	3
163	Malate dehydrogenase, mitochondrial	Mdh2	36 kDa	30
164	Trans-2-enoyl-CoA reductase, mitochondrial	Mecr	40 kDa	5
165	Microsomal glutathione S-transferase 1	Mgst1	18 kDa	6
166	Cob(I)yrinic acid a,c-diamide adenosyltransferase, mitochondrial	Mmab	26 kDa	2
167	MOSC domain-containing protein 2, mitochondrial	Mosc2	38 kDa	8
168	3-mercaptopyruvate sulfurtransferase	Mpst	33 kDa	8
169	39S ribosomal protein L10, mitochondrial	Mrpl10	29 kDa	2
170	39S ribosomal protein L12, mitochondrial	Mrpl12	22 kDa	3
171	28S ribosomal protein S36, mitochondrial	Mrps36	11 kDa	2
172	Mitochondrial carrier homolog 2	Mtch2	33 kDa	7
173	Metaxin-1	Mtx1	36 kDa	2
174	Metaxin-2	Mtx2	30 kDa	11
175	Methylmalonyl-CoA mutase, mitochondrial	Mut	83 kDa	13
176	NADH dehydrogenase [ubiquinone] 1 alpha subcomplex subunit 10, mitochondrial	Ndufa10	41 kDa	2
177	NADH dehydrogenase [ubiquinone] 1 alpha subcomplex subunit 13	Ndufa13	17 kDa	2
178	NADH dehydrogenase [ubiquinone] 1 alpha subcomplex subunit 4	Ndufa4	9 kDa	5
179	NADH dehydrogenase [ubiquinone] 1 alpha subcomplex subunit 6	Ndufa6	15 kDa	2
180	NADH dehydrogenase [ubiquinone] 1 alpha subcomplex subunit 8	Ndufa8	20 kDa	4
181	NADH dehydrogenase [ubiquinone] 1 alpha	Ndufa9	43 kDa	6

	subcomplex subunit 9, mitochondrial			
182	NADH dehydrogenase [ubiquinone] 1 beta subcomplex subunit 10	Ndufb10	21 kDa	5
183	NADH dehydrogenase [ubiquinone] 1 beta subcomplex subunit 11, mitochondrial	Ndufb11	17 kDa	2
184	NADH dehydrogenase [ubiquinone] 1 beta subcomplex subunit 4	Ndufb4	15 kDa	2
185	NADH dehydrogenase [ubiquinone] 1 beta subcomplex subunit 5, mitochondrial	Ndufb5	22 kDa	2
186	NADH dehydrogenase [ubiquinone] 1 beta subcomplex subunit 6	Ndufb6	16 kDa	3
187	NADH dehydrogenase [ubiquinone] 1 beta subcomplex subunit 8, mitochondrial	Ndufb8	22 kDa	2
188	NADH dehydrogenase [ubiquinone] 1 beta subcomplex subunit 9	Ndufb9	22 kDa	2
189	NADH-ubiquinone oxidoreductase 75 kDa subunit, mitochondrial	Ndufs1	80 kDa	7
190	NADH dehydrogenase [ubiquinone] iron-sulfur protein 3, mitochondrial	Ndufs3	30 kDa	3
191	NADH dehydrogenase [ubiquinone] iron-sulfur protein 7, mitochondrial	Ndufs7	25 kDa	2
192	NADH dehydrogenase [ubiquinone] iron-sulfur protein 8, mitochondrial	Ndufs8	24 kDa	2
193	NADH dehydrogenase [ubiquinone] flavoprotein 2, mitochondrial	Ndufv2	27 kDa	2
194	NFU1 iron-sulfur cluster scaffold homolog, mitochondrial	Nfu1	29 kDa	4
195	Nucleoside diphosphate kinase A	Nme1	17 kDa	2
196	NAD(P) transhydrogenase, mitochondrial	Nnt	114 kDa	10
197	Ornithine aminotransferase, mitochondrial	Oat	48 kDa	11
198	OCIA domain-containing protein 1	Ociad1	28 kDa	4
199	2-oxoglutarate dehydrogenase, mitochondrial	Ogdh	116 kDa	45
200	Dynamin-like 120 kDa protein, mitochondrial	Opa1	111 kDa	19
201	Succinyl-CoA:3-ketoacid-coenzyme A transferase 1, mitochondrial	Oxct1	56 kDa	18
202	Propionyl-CoA carboxylase alpha chain, mitochondrial	Pcca	80 kDa	4
203	Propionyl-CoA carboxylase beta chain, mitochondrial	Pccb	58 kDa	3
204	Phosphoenolpyruvate carboxykinase [GTP], mitochondrial	Pck2	71 kDa	9
205	Pyruvate carboxylase, mitochondrial	Pcx	130 kDa	90
206	Pyruvate dehydrogenase E1 component subunit alpha, somatic form, mitochondrial	Pdha1	43 kDa	19
207	Pyruvate dehydrogenase E1 component subunit beta, mitochondrial	Pdhb	39 kDa	16
208	Pyruvate dehydrogenase protein X component, mitochondrial	Pdhx	54 kDa	2
209	Peroxisomal 3,2-trans-enoyl-CoA isomerase	Peci	43 kDa	5
210	Serine/threonine-protein phosphatase PGAM5, mitochondrial	Pgam5	32 kDa	2
211	Prohibitin	Phb	30 kDa	25
212	Prohibitin-2	Phb2	33 kDa	19
213	Presequence protease, mitochondrial	Pitrm1	117 kDa	13
214	Mitochondrial-processing peptidase subunit alpha	Pmpca	58 kDa	3
215	Mitochondrial-processing peptidase subunit beta	Pmpcb	55 kDa	5
216	Polyribonucleotide nucleotidyltransferase 1, mitochondrial	Pnpt1	86 kDa	2
217	Polymerase delta-interacting protein 2	Poldip2	42 kDa	3
218	Thioredoxin-dependent peroxide reductase,	Prdx3	28 kDa	11

	mitochondrial			
219	Peroxiredoxin-5, mitochondrial	Prdx5	22 kDa	9
220	Sulfated glycoprotein 1	Psap	61 kDa	3
221	Prostaglandin E synthase 2	Ptges2	43 kDa	7
222	Polymerase I and transcript release factor	Ptrf	44 kDa	7
223	Peptidyl-tRNA hydrolase 2, mitochondrial	Ptrh2	20 kDa	6
224	Ras-related protein Rab-11B	Rab11B	24 kDa	3
225	Ras-related protein Rab-1B	Rab1B	22 kDa	4
226	Reactive oxygen species modulator 1	Romo1	8 kDa	2
227	Sorting and assembly machinery component 50 homolog	Samm50	52 kDa	7
228	Non-specific lipid-transfer protein	Scp2	59 kDa	6
229	Succinate dehydrogenase [ubiquinone] flavoprotein subunit, mitochondrial	Sdha	73 kDa	22
230	Succinate dehydrogenase [ubiquinone] iron-sulfur subunit, mitochondrial	Sdhb	32 kDa	7
231	Sideroflexin-1	Sfxn1	36 kDa	13
232	Mitochondrial dicarboxylate carrier	Slc25A10	32 kDa	20
233	Mitochondrial 2-oxoglutarate/malate carrier protein	Slc25A11	34 kDa	8
234	Calcium-binding mitochondrial carrier protein Aralar2	Slc25A13	74 kDa	2
235	Mitochondrial carnitine/acylcarnitine carrier protein	Slc25A20	33 kDa	3
236	Mitochondrial glutamate carrier 1	Slc25A22	35 kDa	6
237	Phosphate carrier protein, mitochondrial	Slc25A3	40 kDa	14
238	Adiponectin	Slc25A4	27 kDa	7
239	ADP/ATP translocase 1	Slc25A5	33 kDa	9
240	Superoxide dismutase [Cu-Zn]	Sod1	16 kDa	5
241	Superoxide dismutase [Mn], mitochondrial	Sod2	25 kDa	6
242	SPRY domain-containing protein 4	Spryd4	23 kDa	2
243	Sulfide:quinone oxidoreductase, mitochondrial	Sqrdl	50 kDa	5
244	Single-stranded DNA-binding protein, mitochondrial	Ssbp1	17 kDa	2
245	Stomatin-like protein 2	Stoml2	38 kDa	5
246	Succinyl-CoA ligase [ADP-forming] subunit beta, mitochondrial	Sucla2	50 kDa	10
247	Succinyl-CoA ligase [GDP-forming] subunit alpha, mitochondrial	Suclg1	36 kDa	9
248	Succinyl-CoA ligase [GDP-forming] subunit beta, mitochondrial	Suclg2	47 kDa	8
249	Translational activator of cytochrome c oxidase 1	Taco1	32 kDa	3
250	Mitochondrial import inner membrane translocase subunit Tim13	Timm13	10 kDa	2
251	Mitochondrial import inner membrane translocase subunit Tim17-B	Timm17B	18 kDa	2
252	Mitochondrial import inner membrane translocase subunit Tim23	Timm23	22 kDa	3
253	Mitochondrial import inner membrane translocase subunit TIM44	Timm44	51 kDa	5
254	Mitochondrial import inner membrane translocase subunit TIM50	Timm50	40 kDa	7
255	Mitochondrial import inner membrane translocase subunit Tim8 A	Timm8A1	11 kDa	3
256	Mitochondrial import inner membrane translocase subunit Tim9	Timm9	10 kDa	2
257	Transmembrane protein 126A	Tmem126A	22 kDa	2
258	Trimethyllysine dioxygenase, mitochondrial	Tmlhe	50 kDa	5
259	Mitochondrial import receptor subunit TOM22 homolog	Tomm22	16 kDa	4

260	Mitochondrial import receptor subunit TOM40 homolog	Tomm40	38 kDa	8
261	Mitochondrial import receptor subunit TOM70	Tomm70A	68 kDa	2
262	Tripeptidyl-peptidase 1	Tpp1	61 kDa	2
263	Heat shock protein 75 kDa, mitochondrial	Trap1	80 kDa	15
264	Elongation factor Ts, mitochondrial	Tsfm	35 kDa	4
265	Thiosulfate sulfurtransferase	Tst	33 kDa	6
266	Elongation factor Tu, mitochondrial	Tufm	50 kDa	13
267	Thioredoxin, mitochondrial	Txn2	18 kDa	2
268	Cytochrome b-c1 complex subunit 7	Uqcrb	14 kDa	7
269	Cytochrome b-c1 complex subunit 1, mitochondrial	Uqcrc1	53 kDa	11
270	Cytochrome b-c1 complex subunit 2, mitochondrial	Uqcrc2	48 kDa	15
271	Cytochrome b-c1 complex subunit Rieske, mitochondrial	Uqcrfs1	29 kDa	8
272	Cytochrome b-c1 complex subunit 6, mitochondrial	Uqcrh	10 kDa	2
273	Cytochrome b-c1 complex subunit 8	Uqcrq	10 kDa	4
274	Up-regulated during skeletal muscle growth protein 5	Usmg5	6 kDa	3
275	Voltage-dependent anion-selective channel protein 1	Vdac1	32 kDa	18
276	Voltage-dependent anion-selective channel protein 2	Vdac2	32 kDa	10
277	Voltage-dependent anion-selective channel protein 3	Vdac3	31 kDa	10

Figure 11 A illustrates the mass distribution of the 277 identified mitochondrial proteins. Proteins range from 6 kDa (Usmg5) to 272 kDa (Fasn), though the vast majority detected are lower molecular mass proteins (191 proteins <50 kDa), which corresponds to 68.95% of all detected mitochondrial proteins. The distribution of these proteins to the different compartments of the mitochondrion is shown in Figure 11 B. Most of the proteins belong to the mitochondrial inner membrane (117 proteins). But still, compared to the MitoCarta database, only half of the proteins of the mitochondrial inner membrane could be identified. This is also true for other mitochondrial compartments as the matrix, the intermembrane space or the outer membrane.

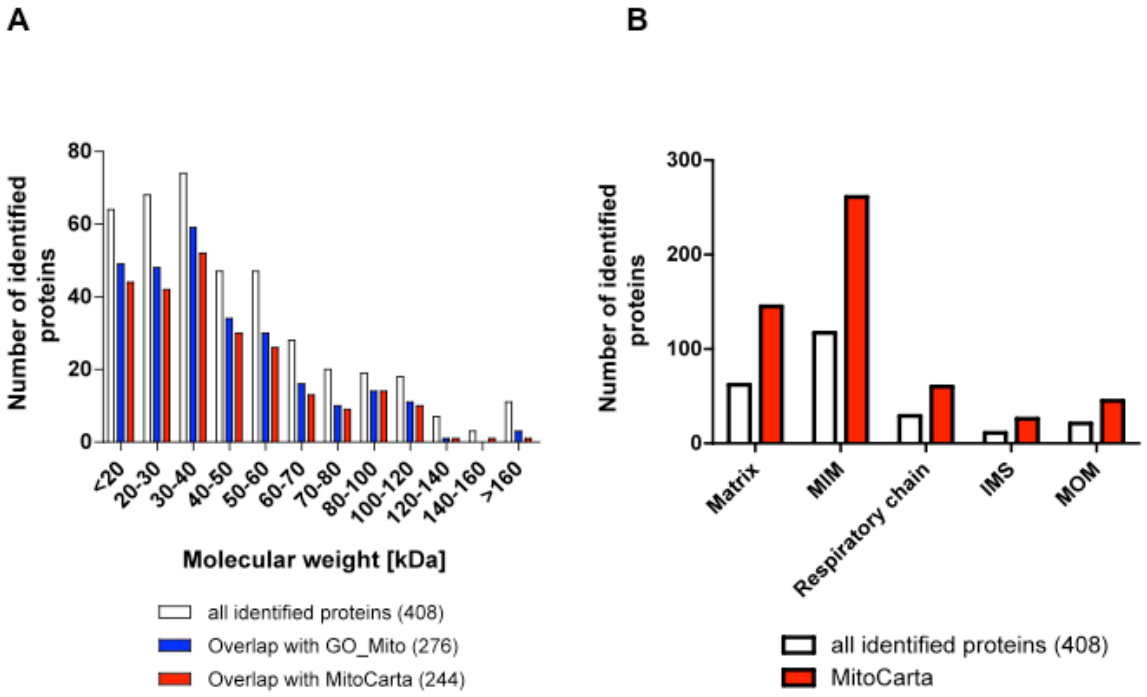

Figure 11 Distribution of isolated mitochondria fractions (A) Molecular mass distribution of the 408 detected proteins in isolated mitochondria fractions (n=8) identified in the spectral counting approach (white bars). Blue and red bars show how many of these proteins of a particular size are ascribed to be mitochondrial according to GO-terms (blue bars) and MitoCarta (red bars) (B) Distribution of identified proteins (white bars) assigned to the mitochondrial matrix, the mitochondrial inner membrane (MIM), the respiratory chain, the intermembrane space (IMS) and the mitochondria outer membrane (MOM). Red bars show proteins identified for these compartments by the MitoCarta Database

A hallmark of the mitochondrial inner membrane is the electron transport chain (ETC) consisting of 5 complexes. An illustration of the ETC and the proteins identified in our approach is given in Figure 12. For complex I (NADH:ubiquinone

oxidoreductase) 18 proteins out of 45 proteins (40%) were identified, for complex II (succinate dehydrogenase) 2 out of 4 (50%), for complex III (ubiquinol:Cytochrome c oxidoreductase) 6 out of 9 (66,6%), for complex IV (Cytochrome c oxidase) 7 out of 17 (41,2%) and for complex V (ATP synthase) 12 out of 19 (63,2%).

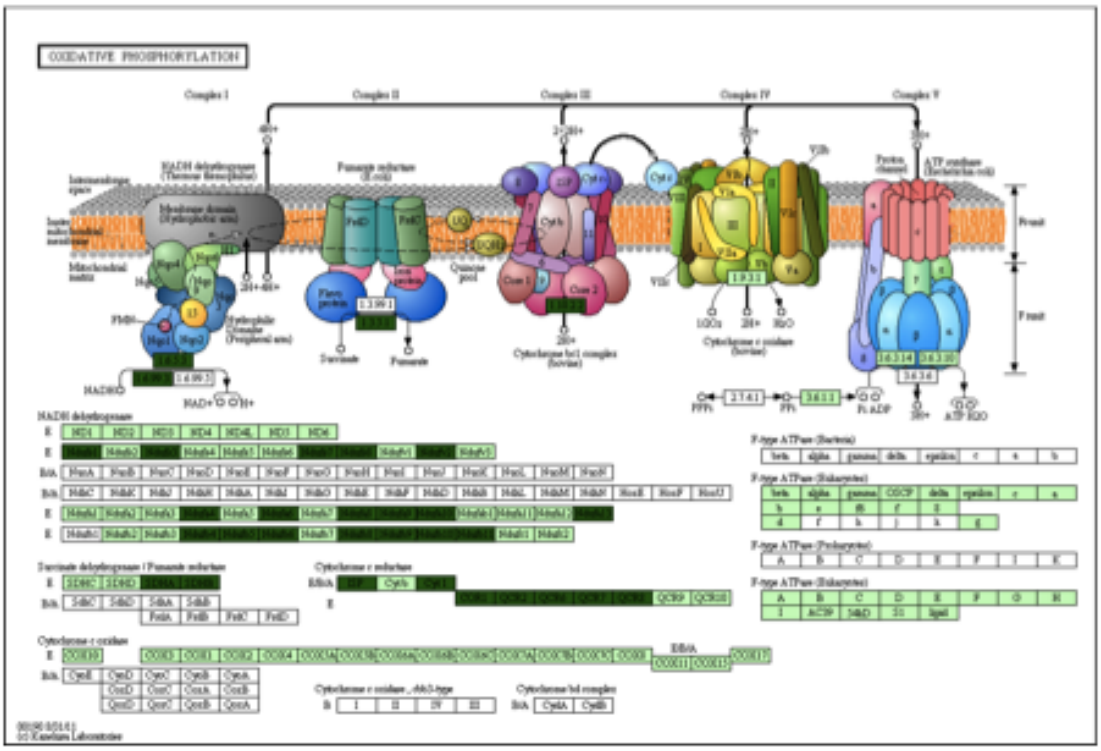

Figure 12 Pathway analysis of oxidative phosphorylation in 3T3-L1 adipocytes mitochondria (http://www.genome.jp/kegg/tool/map_pathway2.html). Proteins in dark green boxes indicate identified proteins, proteins in light green box indicate absence of proteins and proteins in white boxes were not identified in mouse cells.

Another important process that takes place in mitochondria is the citric acid cycle (CAC). All 8 key enzymes of the CAC (exception: Sdhd, Idh3b and Ogdh) and from the pyruvate dehydrogenase complex were detected (shown in table 4-2). Furthermore, we detected the majority of enzymes involved in the FA oxidation pathway (not detected: Acls3 and Cpt1b), also shown in table 4-2. These two processes show a high coverage in our proteomic analysis as indicated by the high number of maximum unique peptides.

Table 4-2 Proteins involved in TCA and FFA Oxidation detected in the proteomic analysis

Protein	Gene name	mol. Mass [kDa]	Max. unique peptides
Citric acid cycle			
aconitase 2, mitochondrial	Aco2	41kDa	5
citrate synthase	Cs	52kDa	22
Dihydrolipoyllysine-residue acetyltransferase component of pyruvate dehydrogenase complex, mitochondrial	Dlat	68kDa	10
dihydrolipoamide S-succinyltransferase (E2 component of 2-oxo-glutarate complex)	Dlst	49kDa	7
fumarate hydratase 1	Fh1	54kDa	16
isocitrate dehydrogenase 2 (NADP+), mitochondrial	Idh2	51kDa	16
isocitrate dehydrogenase 3 (NAD+) alpha	Idh3A	40kDa	21
isocitrate dehydrogenase 3 (NAD+), gamma	Idh3G		12
malate dehydrogenase 1, NAD (soluble)	Mdh1	37kDa	3
malate dehydrogenase 2, NAD (mitochondrial)	Mdh2	36kDa	30
Pyruvate dehydrogenase E1 component subunit alpha, somatic form, mitochondrial	Pdha1	43kDa	19
Pyruvate dehydrogenase E1 component subunit beta, mitochondrial	Pdhb	39kDa	16
Pyruvate dehydrogenase protein X component, mitochondrial	Pdhx	54kDa	2
succinate dehydrogenase complex, subunit A, flavoprotein (Fp)	Sdha	73kDa	22
succinate dehydrogenase complex, subunit B, iron sulfur (Ip); similar to succinate dehydrogenase Ip subunit	Sdhb	32kDa	7
succinate-CoA ligase, GDP-forming, alpha subunit	Suclg1	36kDa	9
succinate-Coenzyme A ligase, ADP-forming, beta subunit	Sucla2	50kDa	10
succinate-Coenzyme A ligase, GDP-forming, beta subunit	Suclg2	47kDa	8
Free fatty acid oxidation			
Acyl-CoA synthetase family member 2, mitochondrial	Acsl1	68kDa	9
Carnitine O-palmitoyltransferase 2, mitochondrial	Cpt2	74kDa	21
Short-chain specific acyl-CoA dehydrogenase, mitochondrial	Acadvl	45kDa	13
Trifunctional enzyme subunit alpha, mitochondrial	Hadha	83kDa	44
Trifunctional enzyme subunit beta, mitochondrial	Hadhb	51kDa	25
Long-chain specific acyl-CoA dehydrogenase, mitochondrial	Acadm	48kDa	19
Medium-chain specific acyl-CoA dehydrogenase, mitochondrial	Acads	46kDa	25
Acyl-CoA-binding protein	Acadsb	10kDa	4
2,4-dienoyl-CoA reductase, mitochondrial	Decr1	36kDa	10
3,2-trans-enoyl-CoA isomerase, mitochondrial	Dci	32kDa	9
Peroxisomal 3,2-trans-enoyl-CoA isomerase	Peci	43kDa	5
Delta(3,5)-Delta(2,4)-dienoyl-CoA isomerase, mitochondrial	Ech1	36kDa	7
Enoyl-CoA hydratase, mitochondrial	Echs1	31kDa	15
Hydroxyacyl-coenzyme A dehydrogenase, mitochondrial	Hadh	34kDa	19
3-hydroxyacyl-CoA dehydrogenase type-2	Hsd17B10	27kDa	13
3-ketoacyl-CoA thiolase, mitochondrial	Acaa2	42kDa	18

4.1.3 Gene Set Enrichment Analysis of the proteomic dataset

Since analysis of differentially expressed genes in SAG-treated 3T3-L1 adipocytes may lead to the generation of a list of genes without any unifying biological significance, we decided to analyse our proteomic dataset by GSEA (http://www.broadinstitute.org/gsea/). Table 4-3 and 4-4 show significant enriched gene sets in 48 hour SAG-treated 3T3-L1 adipocytes with a false discovery rate less or equal 25% (FDR ≤0.25) for unique spectra (L2) and unique peptides (L1), respectively. Figure 13 shows some exemplary enrichment score plots.

Table 4-3 Summary of GSEA results with FDR≤0.25 (L2 – unique spectra list)

Gene set	FDR
C1 – cytogenetic gene sets	
CHR11Q13	0.215
CHR11Q23	0.134
C2 – functional gene sets	
Sweet Lung cancer Kras dn	0.071
Reactome Axon guidance	0.099
Iwanaga Carcinogenesis by Kras PTEN dn	0.100
Mili Pseudopodia haptotaxis dn	0.106
Hollman Apoptosis via CD40 up	0.231
Manalo Hypoxia up	0.231
Reactome Signaling by PDGF	0.222
Liao Metastasis	0.201
Lindgren Bladder cancer cluster 2B	0.190
Moreaux Multiple myeloma by Taci up	0.217
Reactome NCAM signalling for neurite out growth	0.221
Mori Plasma cell up	0.223
Ren Alveolar Rhabdomyosarcoma up	0.213
Reactome NCAM1 interactions	0.207
Creighton Endocrine therapy resistance 3	0.223
Yagi AML with 11Q23 rearranged	0.228
Rutella Response to CSF2RB and IL4 up	0.218
Tarte Plasma cell vs plasmablast up	0.250
Doane Response to androgen dn	0.240
Rodrigues Thyroid carcinoma anaplastic dn	0.233
Lu Aging brain dn	0.230
Liu Prostate cancer dn	0.236
Nakamura Tumor zone peripheral vs central dn	0.237
Mili Pseudopodia chemotaxis dn	0.229
West Adrenocortical tumor dn	0.234
Tarte Plasma cell vs B lymphocyte up	0.250
Browne HCMV infection 18hr dn	0.247
C5 – GO category gene sets	
0 gene sets are significant at FDR < 25%	

Table 4-4 Summary of GSEA results with FDR≤0.25 (L1 – unique peptide list)	
Gene set	**FDR**
C1 – cytogenetic gene sets	
0 gene sets are significant at FDR < 25%	
C2 – functional gene sets	
Mili Pseudopodia haptotaxis dn	0.085
Reactome axon guidance	0.143
Reactome NCAM signalling for neurite out growth	0.217
Hollman Apoptosis via CD40 up	0.228
Liao Metastasis	0.227
Reactome Signalling by PDGF	0.234
Creighton Endocrine therapy resistance 3	0.237
Rutella Response to CSF2RB and IL4 up	0.242
C5 – GO category gene sets	
0 gene sets are significant at FDR < 25%	

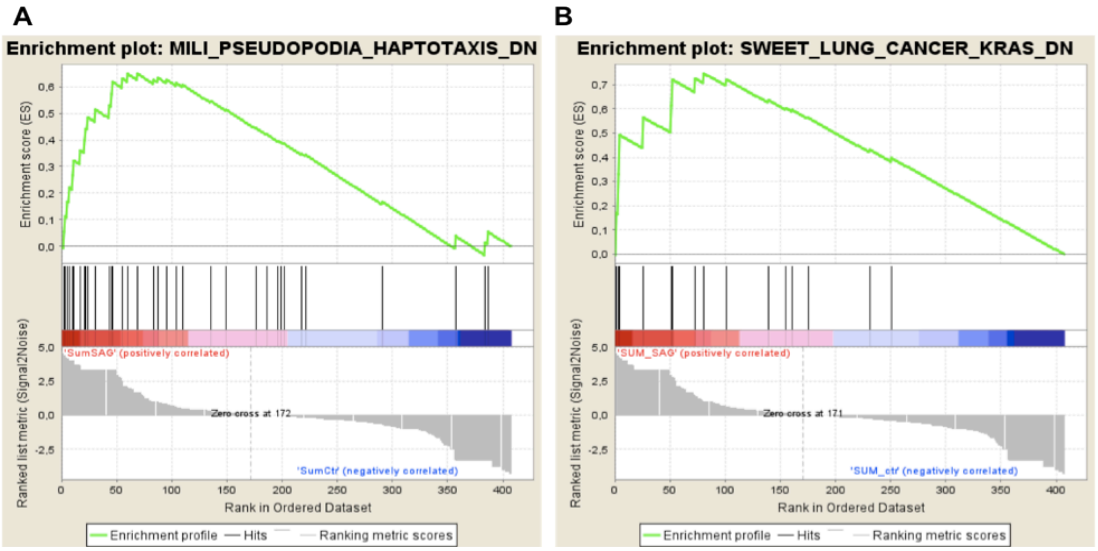

Figure 13 Enrichment score plot showing the ES of the gene set with the smallest FDR for the unique peptide list (A) and for the unique spectra list (B)

4.2 Mitochondrial dynamics is not significantly shifted in SAG treated adipocytes

To gain more insight into the mitochondrial dynamics of SAG-treated 3T3-L1 adipocytes, we performed qPCR of mitochondrial fusion and fission targets, namely Mfn1, Mfn2, Dnm1l, Fis1 and Dctn2. Furthermore, we looked at the induction of nuclear respiratory factor 1 (Nrf1) and mitochondrial transcription factor A (Tfam), both indicators of mitochondrial biogenesis. We could observe shifted mitochondrial dynamics in 3T3-L1 adipocytes treated with SAG for 48 hours compared to control cells. However a significant difference could only be observed in the first experiment for Mfn2 (Fold change: SAG 48 hours: 1.32 ± 0,21/Control 1.00 ± 0.09), shown in Figure 14. This significant difference could not be reproduced in the following experiments. There was also the tendency of an increased expression of Mfn1 and Dctn2, but the fold change never reached significance. Nrf1 also showed a non-significant minor trend towards increased expression. Next, we performed the same set of experiments with 3T3-L1 preadipocytes and again could not observe any significant difference (data not shown).

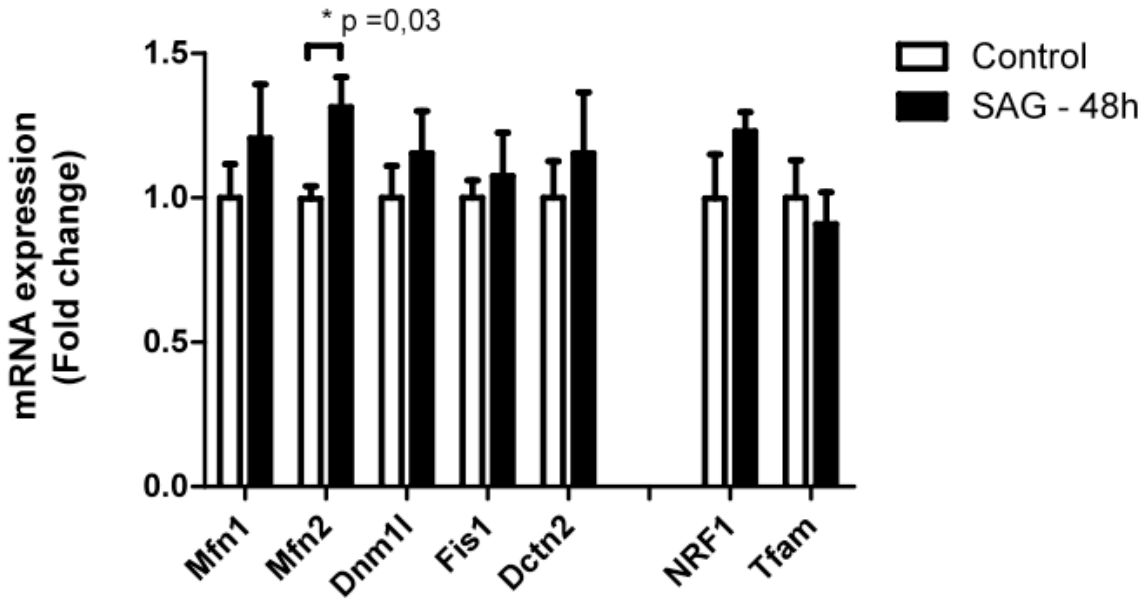

Figure 14 Mitochondrial biogenesis target genes: Mitochondrial fusion and fission genes, nuclear respiratory factor 1 and Tfam mRNA were analysed by means of q-RT-PCR. Only significant difference was observed for Mfn2, but this difference was not persistent throughout all experiments. Mfn1 = mitofusin 1, Mfn2 = mitofusin 2, Dnm1l = dynamin-1-like, Fis1 = fission-1, Dctn2 = dynactin 2, NRF1 = nuclear respiratory factor 1, Tfam = transcription factor A, mitochondrial. Data are shown as mean ± SEM, n=4

4.3 Exposure to SAG is not changing mitochondrial volume and mtDNA content in 3T3-L1 adipocytes

To check if there is a difference in mitochondrial mass between SAG-treated adipocytes and control adipocytes, we performed staining with Mitotracker Green FM. Putative changes were investigated with FACS analysis and confocal microscopy. As is shown in Figure 15 B & C no significant difference could be observed between SAG-treated and control adipocytes after 48 hours of treatment. The same observation was made for 3T3-L1 preadipocytes treated for 48 hours with SAG (data not shown).

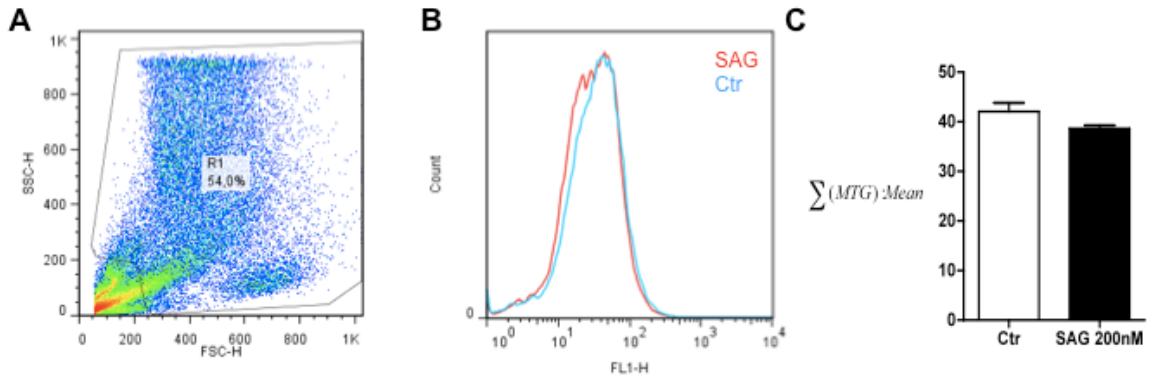

Figure 15 Mitotracker Green FM Fluorescence as an indicator for mitochondrial mass (A) Representation of FSC/SSC of 3T3-L1 adipocytes and gating of cells to exclude debris (B) Histogram of the FL-1 Channel (MTG) showing one representative sample for SAG-treated cells and one representative sample for control cells (C) No significant difference in Mitotracker Green fluorescence could be observed between the SAG-treated group and the control group, Data are shown as mean ± SEM, n=5

The same set of experiments analysed with confocal microscopy confirmed our results obtained from FACS analysis. Figure 16 shows the mitochondrial distribution in 3T3-L1 adipocytes treated with SAG for 48 hours. The same staining (i.e. mitochondrial volume) was obtained with control cells (data not shown).

Next, we measured mtDNA and genomic DNA (gDNA) content by qPCR to obtain an indirect measurement for mitochondrial mass, given by the mtDNA/gDNA ratio. An increase in mitochondrial number would be accompanied with an increase in mitochondrial DNA content, while the genomic DNA content should be unchanged. Thus, this increase in mitochondrial DNA would be reflected in an increased mtDNA/gDNA ratio.

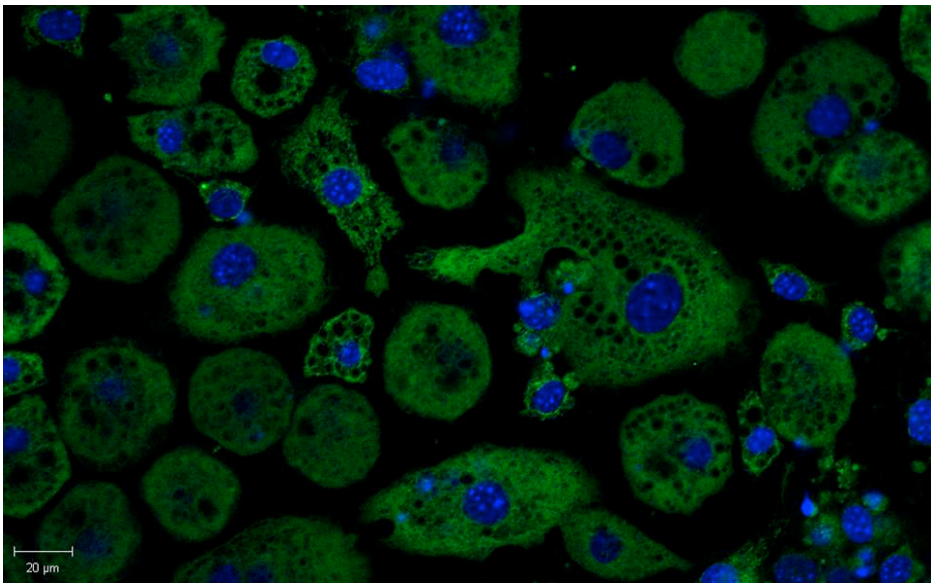

Figure 16 Distribution of mitochondria in 3T3-L1 adipocytes: The mitochondria take up most of the cytoplasmic space of an adipocyte. Lipid droplets and nucleus are clearly evident as they are left out by the mitochondrial meshwork

To amplify mtDNA and gDNA we used primers for the mitochondrial gene NADH-ubiquinone oxidoreductase chain 2 (mtND2) and for the nuclear encoded gene NADH dehydrogenase [ubiquinone] flavoprotein 1 (gNdufv1). We were able to confirm our results from confocal microscopy and the FACS analysis, since we could not see any significant difference in mtDNA/gDNA ratios between the two groups (Figure 17 A). To make sure that these ratios are not the result of an unexpected change in the genomic DNA content we depicted Ct values from the qPCR in Figure 17 B.

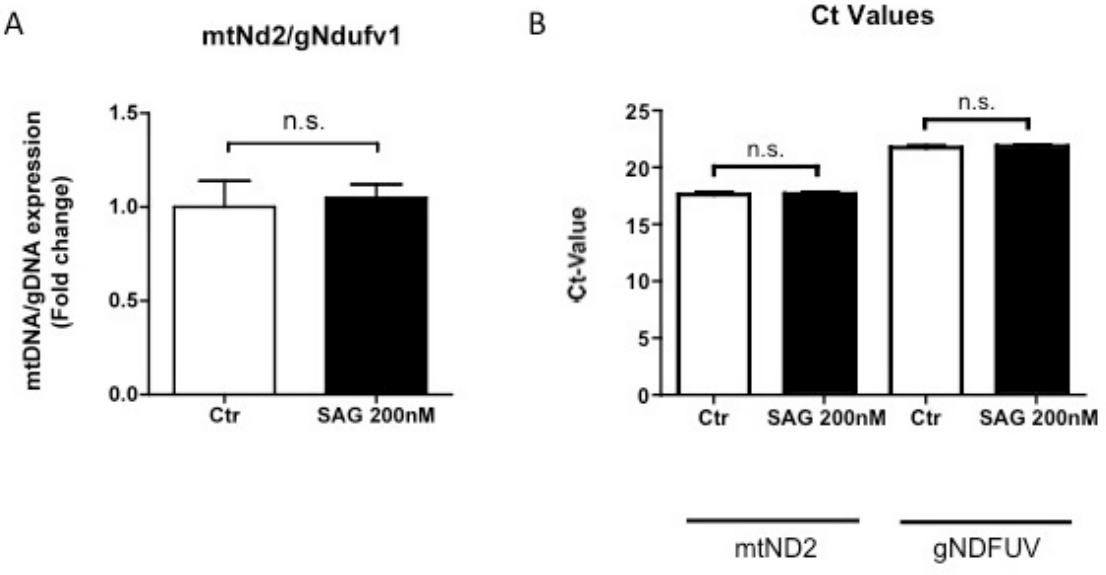

Figure 17 mtDNA/gDNA ratios as an indirect measurement for mitochondrial mass (A) mtDNA/gDNA ratio differences between SAG-treated and control adipocytes (B) Ct-values of mitochondrial and genomic target genes used to establish the mtDNA/gDNA ratio, Data are shown as mean ± SEM, n=4

4.4. Mitochondrial membrane potential (Δψm) is unchanged after exposure to SAG

To investigate the mitochondrial membrane potential (Δψm) of mature adipocytes treated with SAG for 48 hours, we used two techniques: FACS analysis and confocal microscopy. In FACS analysis we evaluated the ratio of cells with a high membrane potential (population R3, Figure 18 B) and cells with a low membrane potential (population R2, Figure 18 B). No difference in this ratio between SAG-treated and control cells could be observed (Figure 18 D). As a control for TMRE staining we used the protonophore FCCP, which decreases the TMRE fluorescence due to depolarization of the mitochondrial membrane (Figure 18 C).

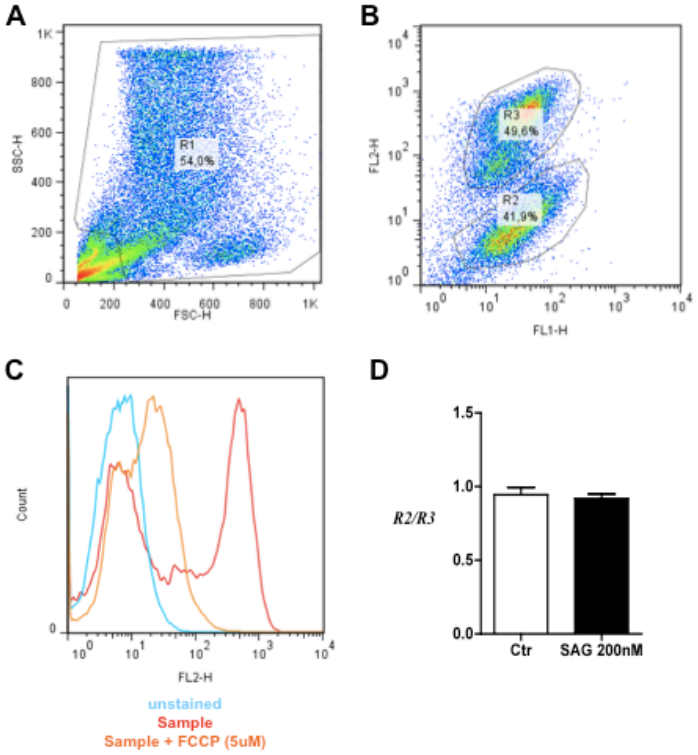

Figure 18 Membrane potential FACS analysis with TMRE
(A) Representation of FSC/SSC of 3T3-L1 adipocytes and gating of cells to exclude debris
(B) Adipocytes stained with TMRE and Mitotracker Green FM show two populations: one population with high membrane potential mitochondria (R3) and one with low membrane potential mitochondria (R2)
(C) Histogram of the FL-2 channel (TMRE) showing the negative control
(D) Ratio of low membrane potential population R2 to high membrane potential population R3 is showing no difference in SAG-treated samples
Data are shown as mean ± SEM, n=5

Furthermore, we evaluated the ratio of TMRE fluorescence to Mitotracker Green fluorescence between the two groups (Figure 19). Since Mitotracker Green stains mitochondria independent of the mitochondrial membrane potential, it is an accepted

approach to normalize membrane potential (TMRE fluorescence) to mitochondrial number (Mitotracker Green fluorescence).

In a set of experiments we observed a significant decrease of TMRE fluorescence in SAG-treated cells (Figure 19 B), but normalized to Mitotracker Green fluorescence this significant decrease abolishes (Figure 19 C). However, the significant decrease in TMRE staining could not be reliably reproduced.

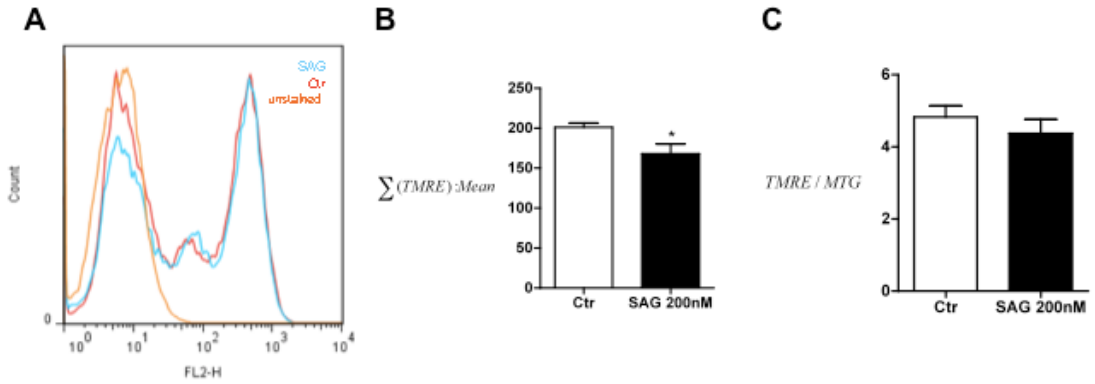

Figure 19 No significant difference in membrane potential status could be observed for SAG-treated adipocytes (A) Histogram of the FL-2 channel (TMRE) showing one representative sample of control cells and one representative sample of SAG-treated cells (B&C) A significant difference in TMRE fluorescence could be observed in SAG-treated adipocytes. TMRE/MTG fluorescence ratios did not differ. Data are shown as mean ± SEM, n=5

Again, confocal microscopy was used to validate our results obtained from FACS measurements. As in FACS analysis we could not find any significant difference between SAG-treated and control cells. An exemplary SAG-treated cell and control cell is depicted in Figures 20 and 21, respectively.

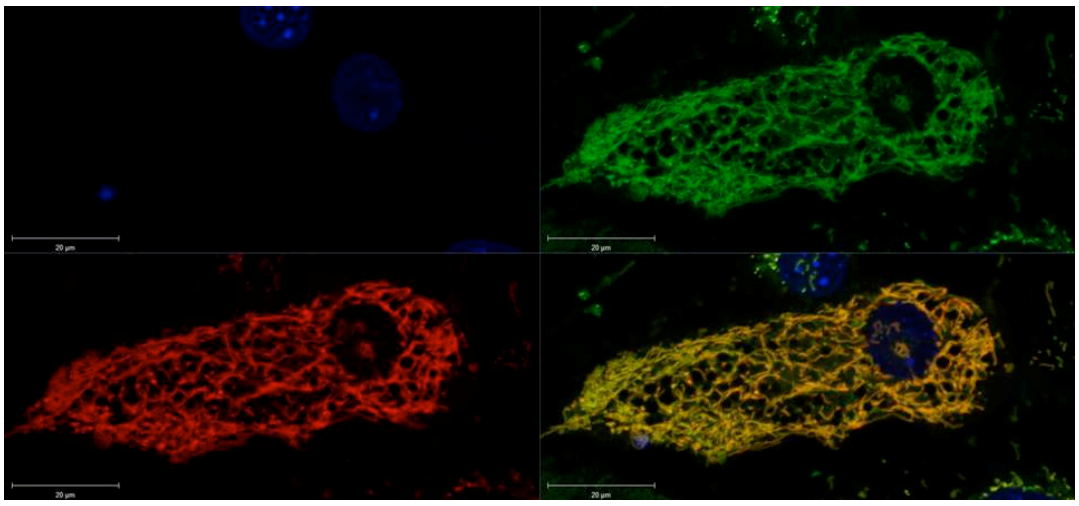

Figure 20 Mitochondrial membrane potential in 3T3-L1 adipocytes treated for 48 hours with SAG – The majority of mitochondria in the adipocyte – regardless of there spatial position – show a strong TMRE staining, reflecting a high membrane potential.

The mitochondrial network spreads out through the whole adipocyte, taking up most of the space of the cytoplasm, only sparing lipid droplets and the nucleus. Of note, there is a homozygous distribution of mitochondria with high membrane potential throughout the cell, both in SAG-treated and control cells.

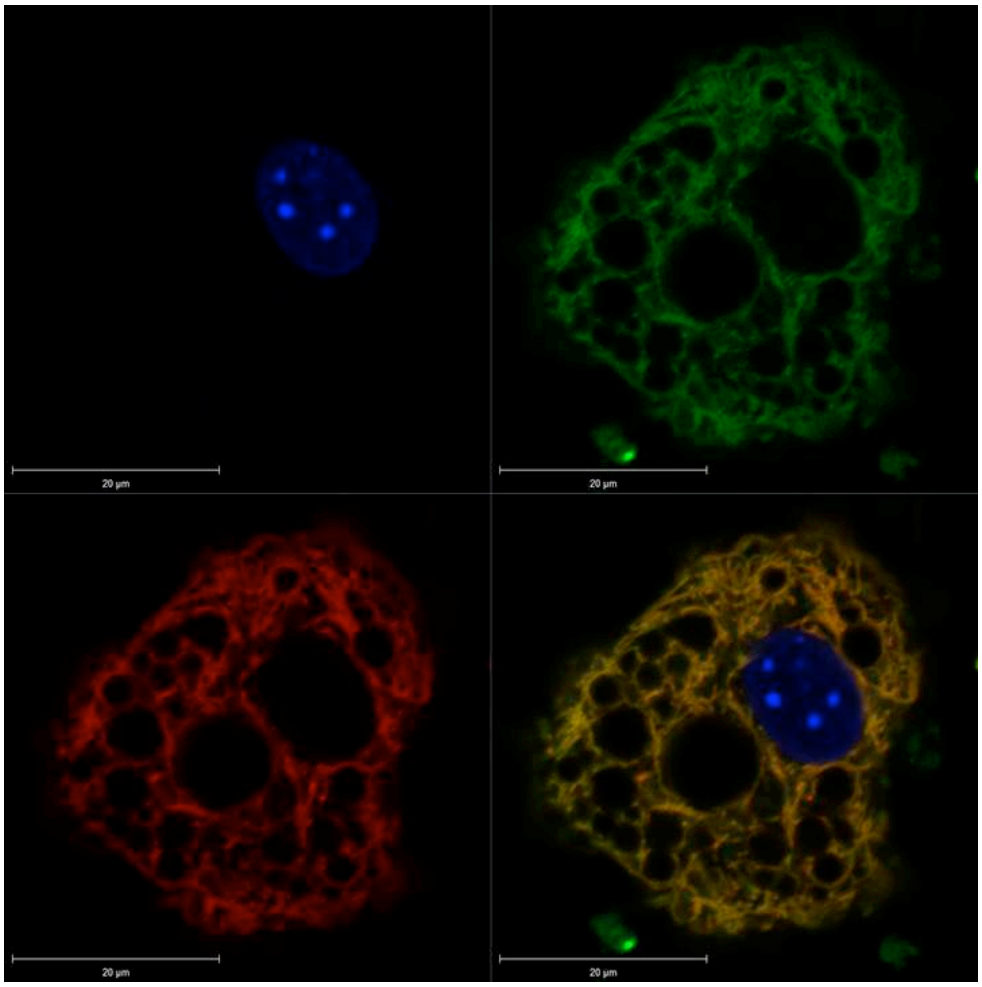

Figure 21 Mitochondrial membrane potential in untreated 3T3-L1 adipocytes As for SAG-treated adipocytes, mitochondria show a strong TMRE staining regardless of their spatial position in control adipocytes

4.5. No change in mitochondrial ultra-structure after exposure to SAG

Finally, we applied electron microscopy to test for differences in mitochondrial morphology, such as shape of mitochondria or density of the mitochondrial cristae, mitochondrial number and distribution in the adipocyte. Since there was no significant difference in mitochondrial distribution and number in SAG-treated and control 3T3-L1 adipocytes, we could confirm our findings from the previous experiments. This was true for 24 hours and 48 hours of SAG-treated adipocytes. Figure 22 illustrates the mitochondrial distribution observed in our 3T3-L1 treated adipocytes. The mitochondria take up most of the cytoplasmic space.

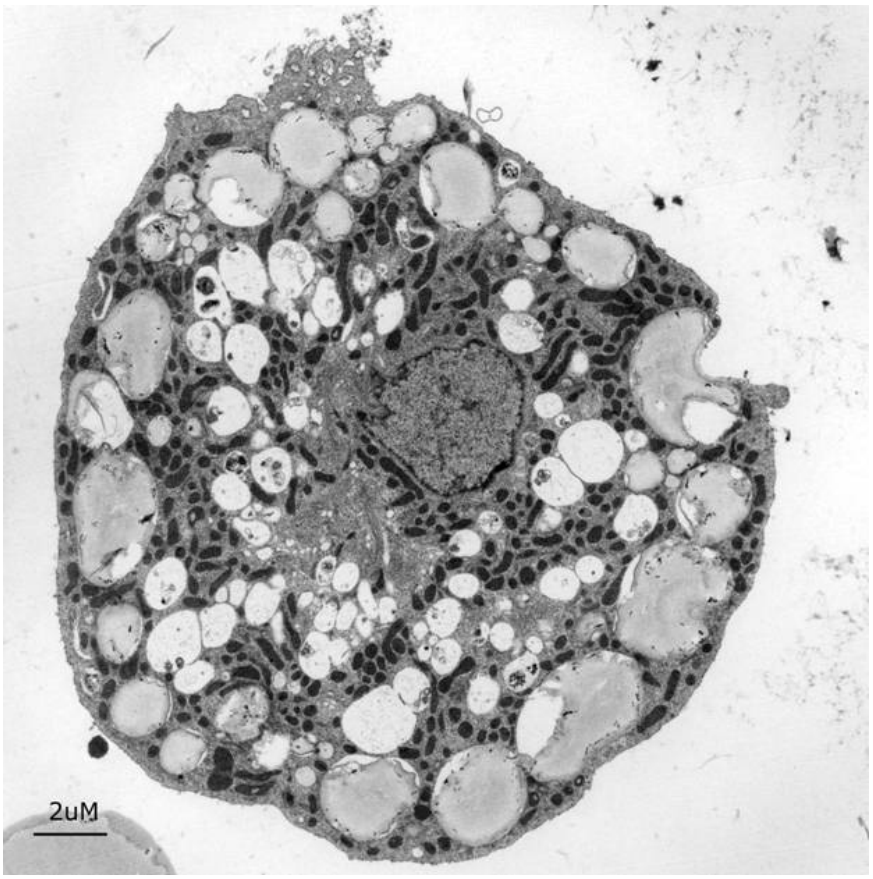

Figure 22 An exemplary picture showing the distribution of mitochondria (small dark elongated and round structures) in a SAG-treated 3T3-L1 adipocyte. They take up most of the cytoplasmic space besides fat droplets (white and grey round structures). x2000 magnification

Electron microscopy pictures of higher magnification did not reveal any significant differences in ultra-structure such as the density of the mitochondrial cristae or the inner membrane (Figures 23 A-D).

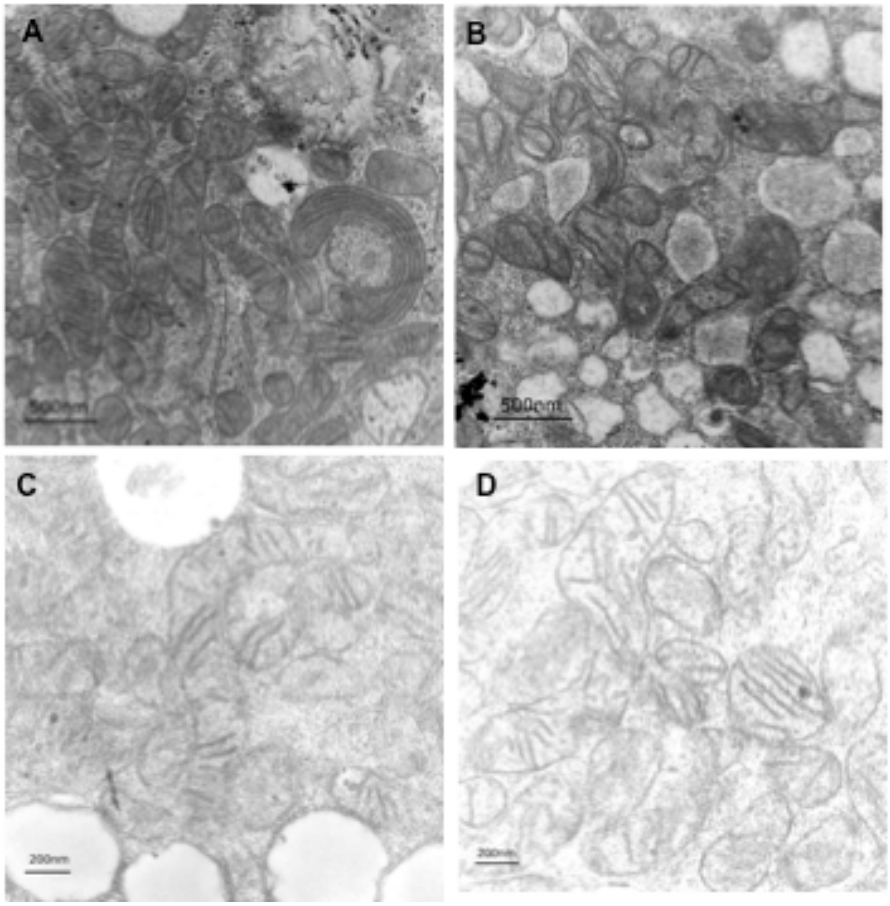

Figure 23 Mitochondrial ultrastructure in 24 hours and 48 hours SAG-treated 3T3-L1 adipocytes (A) 24 hours treated control 3T3-L1 adipocyte, x12.000 magnification (B) 24 hours SAG-treated 3T3-L1 adipocyte, x12.000 magnification (C) 48 hours treated control 3T3-L1 adipocytes, x20.000 magnification (D) 48 hours SAG-treated adipocytes, x20.000 magnification

5. DISCUSSION

Focus of our attention was the establishment of a mitochondrial proteomic approach that makes it possible to compare the mitochondrial proteome of SAG-treated 3T3-L1 mature adipocytes to untreated control cells. In our study we decided to isolate crude mitochondrial fractions and exclude non-mitochondrial proteins from our protein list using bioinformatics filtering. Therefore, we compared our final protein list, encompassing 408 proteins in total (SAG treated plus untreated controls), with MitoCarta and Gene ontology terms. This approach resulted in a protein list with a total of 277 mitochondrial proteins. In general, there are three crucial factors to get satisfying results in mitochondrial proteomics. The first crucial factor is the starting material. Losses will be more severe and mitochondrial purity will suffer if the preparation starts with small amounts of cells. Thus, we started our proteomic approach with a total of sixteen 150 cm^2 cell culture flasks. Two flasks were always combined to obtain one biological sample, thus ending up with quadruplicates (4 SAG treated vs. 4 control samples). Another crucial step in the preparation is whether to decide to isolate crude or purified mitochondrial fractions. Crude mitochondrial fractions are contaminated with the endoplasmatic reticulum and lysosomes. The contamination of various high abundant non-mitochondrial proteins might mask the MSMS-signal of low abundant mitochondrial proteins. On the other hand, the isolation of highly purified mitochondria by high-speed gradient centrifugation needs high amounts of starting material. In our study we decided to obtain crude mitochondria by differential centrifugation. We tried to optimize this procedure by varying the number of low speed centrifugation steps (1200 g). We have found that additional low speed steps improved the purity of mitochondrial fractions. However, this also reduced total yield. In preparations with less low speed centrifugation steps we detected more proteins in total, sometimes even more mitochondrial proteins. But these mitochondrial fractions were not as pure, thus there were more non-mitochondrial proteins. Additional crucial factors affecting the quality of mitochondrial protein and peptide preparations are the choice of how to solubilize the proteins and the decision whether it is necessary to perform an in-gel or an in-solution digest.

To our knowledge there are two studies that deal with the mitochondrial proteome of differentiated 3T3-L1 adipocytes. The first one performed by Matthias Mann's lab identified 1731 proteins in their highly purified mitochondrial fraction. The second study by Newton et al[114] investigated the mitochondrial proteome during the differentiation of 3T3-L1 adipocytes and could identify a total of 631 proteins in their crude mitochondrial fraction. 288 of these 631 proteins were assigned to be mitochondrial. This study used the same strategy as we did. Thus it is possible to make some simple comparisons. Despite the fact that Newton et al. started with less starting material they were able to identify more proteins in their subsequent MSMS analyses. However, their crude mitochondrial fraction was not as pure as our mitochondrial fraction. An explanation for this might be that they performed less low speed centrifugation steps, and therefore identified more proteins in total at the expense of purity.

Besides the establishment of the mitochondrial proteomic approach, we focused our attention on the evaluation of certain properties of mitochondria following the treatment with the smoothened agonist SAG. Though sometimes we could observe changes, they never reached any significance. To determine the effects of hedgehog signalling on mitochondrial biogenesis/mass, we combined Mitotracker Green FM measurements by FACS as wells as confocal microscopy with quantitative measurements of mtDNA/gDNA ratios as an indirect marker of mitochondrial mass. In both experimental settings we could not observe any change in mitochondrial mass. To gain insight into the dynamics of mitochondria we performed RNA measurements of key mitochondrial fission and fusion genes. Though we could observe a slightly shifted dynamics, this never reached any significance.

Another important feature of mitochondria is their membrane potential since it is a key indicator of cell viability. We investigated this property of mitochondria with the cell-permeant cationic dye TMRE by FACS and confocal microscopy. In both experiments we could not see any significant change in the membrane potential in 48 hours SAG treated adipocytes. However, it has to be kept in mind that our live cell imaging approach was far from optimal, since our confocal microscope was missing the necessary temperature-controlled CO_2 humidified chamber. Since the equilibrium of the mitochondrial membrane potential is pH-sensitive we had to investigate our cells immediately after the treatment and maintain them in a buffered media.

Finally, we studied mitochondrial morphology and ultrastructure using electron microscopy. As with all other tests mentioned above, we could not observe any obvious differences between treated and untreated adipocytes.

Taken together, our attempt to identify differences in the mitochondrial compartment of smoothened (i.e. hedgehog signalling) activated mouse adipocytes was unsuccessful. However, due to the technical limitations of our study - i.e. suboptimal equipment used in our approach - this does not necessarily rule out that such differences still exist. To reinvestigate this differences in a more sophisticated manner it will be important to use temperature controlled chambers in all life cell imaging FACS experiments. Furthermore, and most importantly, a quantitative proteomics approach based on stable isotope labelling or similar methods will be necessary to ultimately answer the question whether hedgehog signalling impacts mitochondrial function in 3T3-L1 adipocytes.

6. REFERENCES

[1] Wallace DC A mitochondrial paradigm of metabolic and degenerative diseases, aging , and cancer: A dawn for evolutionary medicine *Annu. Rev. Genet.* **39**, 359-407 (2005)

[2] Mitchell P Chemiosmotic coupling in oxidative and photosynthetic phosphorylation *Glynn Research Ltd*., Bodmin (1966)

[3] Hock MB, Kralli A. Transcriptional Control of Mitochondrial Biogenesis and Function, *Annu. Rev. Physiol*. **71**, 177-203 (2009)

[4] Bleazard W et al The dynamin-related GTPase Dnm1 regulates mitochondrial fission in yeast *Nat. Cell Biol.* **1**, 298-304 (1999)

[5] Labrousse AM et al C. elegans dynamin-related protein DRP-1 controls severing of the mitochondrial outer membrane *Mol. Cell* **4**, 815-826 (1999)

[6] Sesaki H & Jensen RE Division versus fusion: Dnm1p and Fzo1p antagonistically regulate mitochondrial shape *J. Cell Biol*. **147**, 699-706 (1999)

[7] Smirnova E et al Dynamin-related protein Drp1 is required for mitochondrial division in mammalian cells *Mol. Biol. Cell* **12**, 2245-2256 (2001)

[8] Chen H et al. Mitofusin Mfn1 and Mfn2 coordinately regulate mitochondrial fusion and are essential for embryonic development *J. Cell Biol.* **160**, 189-200 (2003)

[9] Hermann GJ et al. Mitochondrial fusion in yeast requires the transmembrane GTPase Fzo1p *J. Cell Biol.* **143**, 359-373 (1998)

[10] Koshiba T et al. Structural basis of mitochondrial tethering by mitofusion complexes *Science* **305**, 858-862 (2004)

[11] Rapaport D et al Fzo1p is a mitochondrial outer membrane protein essential fort he biogenesis of functional mitochondria in Saccharomyces cerevisiae *J. Biol. Chem.* **273**, 20150-20155 (1998)

[12] Wong ED et al The dynamin-related GTPase, Mgm1p, is an intermembrane space protein required for maintainance of fusion competent mitochondria *J. Cell Biology* **151**, 341-352 (2000)

[13] Olichon A et al Loss of OPA1 pertubates the mitochondrial inner membrane structure and integrity, leading to cytochrome c release and apoptosis *J. Cell Biology* **278**, 7743-7746 (2003)

[14] Cipolat S et al OPA1 requires mitofusin 1 to promote mitochondrial fusion *Proc. Natl Acad. Sci. USA* **101**, 15927-15932 (2004)

[15] Meeusen S et al Mitochondrial inner-membrane fusion and cristae maintenance requires the dynamin-related GTPase Mgm1 *Cell* **127**, 383-395 (2006)

[16] Meeusen S et al Mitochondrial fusion intermediates revealed in vitro *Science* **305**, 1747-1752 (2004)

[17] Griffin EE et al. The WD40 protein Caf4p is a component of the mitochondrial fission machinery and recruits Dnm1p to mitochondria *J. Cell Biol.* **170**, 237-248 (2005)

[18] Mozdy AD et al. Dnm1p GTPase-mediated mitochondrial fission is a multi-step process requiring the novel intergral membrane component Fis1p *J. Cell Biol.* **151**, 367-380 (2000)

[19] Okamoto K & Shaw JM Mitochondrial morphology and dynamics in yeast and multicellular eukaryotes *Annu. Rev. Genet.* **39**, 503-536 (2005)

[20] Tieu Q et al. The WD repeat protein, Mdv1p, functions as a molecular adaptor by interacting with Dnm1p and Fis1p during mitochondrial fission *J. Cell Biol.* **158**, 445-452 (2002)

[21] Mozdy AD et al Dnm1p GTPase-mediated mitochondtrial fission is a multi-step process requiring the novel integral membrane component Fis1p *J. Cell Biology* **151**, 367-380 (2000)

[22] Tieu Q et al Mdv1p is a WD reapeat protein that interacts with the dynamin-related GTPase, Dnm1p, to trigger mitochondrial division *J. Cell Biology* **151**, 353-366 (2000)

[23] Lee YJ et al. Roles of the mammalian mitochondrial fission and fusion mediators Fis1, Drp1, and Opa1 in apoptosis *Mol. Biol. Cell* **15**, 5001-5011 (2004)

[24] Smirnowa E et al A human dynamin-related protein controls the distribution of mitochondria *J. Cell Biology* **143**, 351-358 (1998)

[25] Otsuga D et al The dynamin-related GTPase, Dnm1p, controls mitochondrial morphology in yeast *J. Cell Biology* **143**, 333-349 (1998)

[26] Chen H et al Disruption of fusion results in mitochondrial heterogeneity and dysfunction *J. Biol. Chem.* **280**, 26185-26192 (2005)

[27] Frank S et al The role of dynamin-related protein 1, a mediator of mitochondrial fission, in apoptosis *Dev. Cell* **1**, 515-525 (2001)

[28] Pagliarini DJ et al A mitochondrial protein compendium elucidates complex I disease biology *Cell* **134**, 112-123 (2008)

[29] Chow LS et al Impact of endurance training on murine spontaneous activity, muscle mitochondrial DNA abundance, gene transcripts, and function *J. Appl. Physiol.* **102**, 1078-1089 (2007)

[30] Civitarese AE et al Calorie restriction increases muscle mitochondria biogenesis in healthy humans *PLoS Med.* **4**, e76 (2007)

[31] Scarpulla RC et al Transcriptional paradigms in mammalian mitochondrial biogenesis and function *Physiol. Rev.* **88**, 611-638 (2008)

[32] Mootha VK et al Integrated analysis of protein composition, tissue diversity, and gene regulation in mouse mitochondria *Cell* **115**, 629-640 (2003)

[33] Cam H et al A common set of gene regulatory networks links metabolism and growth inhibition *Mol. Cell* **16**, 399-411 (2004)

[34] Wang C et al Cyclin D1 repression of nuclear respiratory factor 1 integrates nuclear DNA synthesis and mitochondrial function *Proc. Natl. Acad. Sci. USA* **103**, 11567-11572 (2006)

[35] Dhar SS et al Nuclear respiratory factor 1 regulates all ten nuclear-encoded subunits of cytochrome c oxidase in neurons *J. Biol. Chem.* **283**, 3120-3129 (2008)

[36] Wu Z et al Mechanisms controlling mitochondrial biogenesis and respiration through the thermogenic coactivator PGC-1 *Cell* **98**, 115-124 (1999)

[37] Andersson U et al Pgc-1-related coactivator, a novel, serum-inducible coactivator of nuclear respiratory factor 1-dependent transcription in mammalian cells *Mol. Cell Biol.* **21**, 3738-3749 (2001)

[38] Lin J et al Peroxisome proliferator-activated receptor γ coactivator 1β (PGC-1β), a novel PGC-1-related transcription coactivator associated with host cell factor *J. Biol. Chem.* **277**, 1645-1648 (2002)

[39] Sakamaki T et al Cyclin D1 determines mitochondrial function in vivo *Mol. Cell Biol.* **26**, 5449-5469 (2006)

[40] Murakami T et al Induction of nuclear respiratory factor-1 expression by an acute bout of exercise in rat muscle *Biochim. Biophys. Acta* **1381**, 113-122 (1998)

[41] Baar K et al Adaptions of skeletal muscle to exercise: rapid increase in the transcriptional coactivator PGC-1 *FASEB J* **16**, 1879-1886 (2002)

[42] McClelland GB Temperature- and exercise-induced gene expression and metabolic enzyme changes in skeletal muscle of adult zebrafish (Danio rerio) *J. Physiol.* **577**, 739-751 (2006)

[43] Bergeron R et al Chronic activation of AMP kinase results in NRF-1 activation and mitochondrial biogenesis *Am. J. Physiol. Endocrinol. Metab.* **281**, E1340-1346 (2001)

[44] Virbasius JV et al Identity of GABP with NRF-2, a multisubunit activator of cytochrome oxidase expression, reveals a cellular role for an ETS domain activator of viral promotors *Genes Dev.* **7**, 380-392 (1993)

[45] Ongwijitwat S et al Nuclear respiratory factor 2 senses changing cellular energy demands and ist silencing down-regulates cytochrome oxidase and other target gene mRNAs *Gene* **374**, 39-49 (2006)

[46] Taylor RW, Turnball DM. Mitochondrial DNA mutations in human disease *Nature Reviews* **6**, 389-402 (2005)

[47] Chinnery PF Searching for nuclear-mitochondrial genes *Trends Genet.* **19**, 60-62 (2003)

[48] DiMauro S, Davidzon G Mitochondrial DNA and disease *Ann. Med.* **37**, 222-232 (2005)

[49] Kirby DM, Thorburn DR, Approaches to Finding the Molecular Basis of Mitochondrial Oxidative Phosphorylation Disorders *Twin Res. Hum. Gen*. **11**, 395-411 (2008)

[50] DiMauro S, Schon EA Mitochondrial respiratory-chain diseases *N. Engl. J. Med.* **348**, 2656-2668 (2003)

[51] Pancrudo J et al Mitochondrial myopathy associated with a novel mutation in mtDNA *Neuromuscul. Disord.* **17**, 651-654 (2007)

[52] Taylor RW et al Catastrophic presentation of mitochondrial disease due to a mutation in the tRNA(His) gene *Neurology* **62**, 1420-1423 (2004)

[53] Calvo SE, Mootha VK. The Mitochondrial Proteome and Human Disease *Annu. Rev. Genomics Hum. Genet.* **11**, 25-44 (2010)

[54] Ingham PW, McMahon AP Hedgehog signaling in animal development: paradigms and principles *Genes Dev.* **15**, 3059-3087 (2001)

[55] Briscoe J, Ericson J Specification of neuronal fates in the ventral neural tube *Curr. Opin. Neurobiol.* **11**, 43-49 (2001)

[56] Ahn S, Joyner AL Dynamic changes in the response of cells to positive hedgehog signaling during mouse limb patterning *Cell* **118**, 505-516 (2004)

[57] Harfe BD et al Evidence for an expansion-based temporal Shh gradient in specifying vertebrate digit identities *Cell* **118**, 517-528 (2004)

[58] Wada H, Makabe K Genome duplications of early vertebrates as a possible chronicle of the evolutionary history of the neural crest *Int. J. Biol. Sci.* **2**, 133-141 (2006)

[59] Echelard SC et al Sonic hedgehog, a member of a family of putative signaling molecules, is implicated in the regulation of CNS polarity *Cell* **75**, 1417-1430 (1993)

[60] Varjosalo M, Taipale J Hedgehog signaling *J. Cell Sci.* **120**, 3-6 (2007)

[61] Varjosalo M, Taipale J Hedgehog: functions and mechanisms *Genes Dev.* **22**, 2454-2472 (2008)

[62] Wang Y, McMahon AP, Allen BL Shifting paradigms in Hedgehog signaling *Curr. Opin. Cell Biol.* **19**(2), 159-165 (2007)

[63] Sampath K et al Functional differences among Xenopus nodal-related genes in left-right axis determination *Development* **124**, 3293-3302 (1997)

[64] Pagan-Westphal SM, Tabin CJ The transfer of left-right positional information during chick embryogenesis *Cell* **93**, 25-35 (1998)

[65] Schilling TF et al Regulation of left-right asymmetries in the zebrafish by Shh and BMP4 *Dev. Biol.* **210**, 277-287 (1999)

[66] Waranabe Y, Nakamura H Control of chicken tectum territory along dorsoventral axis by Sonic hedgehog *Development* **127**, 1131-1140 (2000)

[67] Meyer NP, Roelink H The amino-terminal region of Gli3 antagonizes the Shh response and acts in dorsoventral fate specification in the developing spinal cord *Dev. Biol.* **257**, 343-355 (2003)

[68] Lee JJ et al Autoproteolysis in hedgehog protein biogenesis *Science* **266**, 1528-1537 (1994)

[69] Porter JA et al Cholesterol modification of hedgehog signaling proteins in animal development *Science* **274**, 255-259 (1996)

[70] Chamoun Z et al Skinny hedgehog, an acyltransferase required for palmitoylation and activity of the hedgehog signal *Science* **293**, 2080-2084 (2001)

[71] Burke R et al Dispatched, a novel sterol-sensing domain protein dedicated to the release of cholesterol-modified hedgehog from signaling cells *Cell* **99**, 803-815 (1999)

[72] Mimeault M, Batra SK Frequent deregulation in the hedgehog signaling network and cross-talk with the epidermal growth factor receptor pathway involved in cancer progression and targeted therapies *Pharmacol. Rev.* **62**(3), 497-524 (2010)

[73] Ma Y et al Hedgehog-mediated patterning of the mammalian embryo requires transporter-like function of dispatched *Cell* **111** (1), 63-75 (2002)

[74] The I et al Hedgehog movement is regulated through tout velu-dependent sythesis of a heparan sulfate proteoglycan *Mol. Cell* **4**, 633-639 (1999)

[75] Zhu AJ, Scott MP Incredible journey: how do developmental signals travel through tissue? *Genes Dev.* **18**, 2985-2997 (2004)

[76] Lum L et al Identification of Hedgehog pathway components by RNAi in Drosophila cultured cells *Science* **299**, 2039-2045 (2003)

[77] Tenzen T et al The cell surface membrane proteins Cdo and Boc are components and targets of the Hedgehog signalig pathway and feedback network in mice *Dev. Cell* **10**, 647-656 (2006)

[78] Yao S et al The iHog cell surface proteins bind Hedgehog and mediate pathway activation *Cell* **125**, 343-357 (2006)

[79] Taipale J et al Patched acts catalytically to suppress the activity of Smoothened *Nature* **418**, 892-897 (2002)

[80] Stone DM et al The tumorsuppressor gene patched encodes a candidate receptor for Sonic hedgehog *Nature* **384**, 129-134 (1996)

[81] Lum L, Beachy PA The Hedgehog response network: sensors, switches, and routers *Science* **304**, 1755-1759 (2004)

[82] Matise MP, Joyner AL Gli genes in development and cancer *Oncogene* **18**, 7852-7859 (1999)

[83] Denef N et al Hedgehog induces opposite changes in turnover and subcellular localization of patched and smoothened *Cell* **102**, 512-531 (2000)

[84] Incardona JP et al Sonic hedgehog induces the segregation of patched and smoothened in endosomes *Curr. Biol.* **12**, 983-995 (2002)

[85] Riobo NA, Manning DR Pathways of signal transduction employed by vertebrate Hedgehogs *Biochem. J.* **403**(3), 369-379 (2007)

[86] Svard J et al Genetic elimination of Suppressor of fused reveals an essential repressor function in the mammalian Hedgehog signaling pathway *Dev. Cell* **10**, 187-197 (2006)

[87] Rohatgi R, Scott MP Patching the gaps in Hedgehog signalling *Nat. Cell Biol.* **9**, 1005-1009 (2007)

[88] Cooper MK et al Teratogen-mediated inhibition of target tissue response to Shh signaling *Science* **280**, 1603-1607 (1998)

[89] Corcoran RB, Scott MP Oxysterols stimulate Sonic hedgehog signal transduction and proliferation of medulloblastoma cells *Proc. Natl. Acad. Sci. USA* **103**, 8408-8413 (2006)

[90] Bijlsma MF et al Repression of Smoothened by Patched-dependent (Pro-) Vitamin D3 Secretion *PLoS Biol.* **4**, e282 (2006)

[91] Chen JKet al Small molecule modulation of Smoothened activity *Proc. Natl. Acad. Sci.* **99**, 14071-14076 (2002)

[92] Stanton BZ et al A small molecule that binds Hedgehog and blocks its signaling in human cells *Nat. Chem. Biol.* **5**, 154-156 (2009)

[93] Chen T et al Identification of small-molecule inhibitors of the JIP-JNK interaction *Biochem. J.* **420**, 283-294 (2009)

[94] Huangfu D et al Hedgehog signalling in the mouse requires intraflagellar transport proteins *Nature* **426**, 83-87 (2003)

[95] Nybakken K et al A genome-wide RNA interference screen in Drosophila melanogaster cells for new components of the Hh signaling pathway *Nat. Genet.* **37**, 1323-1332 (2005)

[96] Sun Z et al A genetic screen in zebrafish identifies cilia genes as a principle cause of cystic kidney *Development* **131**, 4085-4093 (2004)

[97] Haycraft CJ et al Gli2 and Gli3 localize to cilia and require the intraflagellar transport protein polaris for processing and function *PLoS Genet.* **1**, e53 (2005)

[98] Corbit KC et al Vertebrate Smoothened functions at the primary cilium *Nature* **437**, 1018-1021 (2005)

[99] Rohatgi R et al Patched1 regulates hedgehog signaling at the primary cilium *Science* **317**, 372-376 (2007)

[100] Ahima RS Digging deeper into obesity *J. Clin. Invest.* **121** (6) 2076-2079 (2011)

[101] World health organization Obesity and overweight WHO website http://www.who.int/mediacentre/factsheets/fs311/en/ updated March 2011, accessed January 2012

[102] Gregor MF, Hotamisligil GS Inflammatory mechanisms in obesity *Annu. Rev. Immunol.* **29**, 415-445 (2011)

[103] Rosen ED, Spiegelman BM Adipocytes as regulators of energy balance and glucose homeostasis *Nature* **444**, 847-853 (2006)

[104] Balistreri CR et al The role of adipose tissue and adipokines in obesity-related inflammatory diseases *Mediators Inflamm.* **2010**, 802078 (2010)

[105] Hotamisligil GS et al Adipose expression of tumor necrosis factor-alpha: direct role in obesity-linked insulin resistance *Science* **259**, 87-91 (1993)

[106] Hotamisligil GS et al Increased adipose tissue expression of tumor necrosis factor-α in human obesity and insulin resistance *J. Clin. Invest.* **95**, 2409-2415 (1995)

[107] Xu H et al Chronic inflammation in fat plays a crucial role in the development of obesity-related insulin resistance *J. Clin. Investig.* **112**, 1821-1830 (2003)

[108] Weisberg SP et al Obesity is associated with macrophage accumulation in adipose tissue *J. Clin. Investig.* **112**, 1796-1808 (2003)

[109] Kopelman PG Obesity as a medical problem *Nature* **404**, 635- 643 (2000)

[110] Ahima RS Digging deeper into obesity *J Clin Invest* **121**, 2076-2079 (2011)

[111] Pospisilik JA et al Drosophila genome-wide obesity screen reveals Hedgehog as a determinant of brown versus white adipose cell fate *Cell* **140**, 148-160 (2010)

[112] Warburg O On the origin of cancer cells *Science* **123**, 309-314 (1956)

[113] A Subaramanian et al Gene set enrichment analysis: A knowlegde-based approach for interpreting genome-wide expression profiles PNAS 2005

[114] Newton BW et al Proteomic analysis of 3T3-L1 adipocyte mitochondria during differentiation and enlargement *J. Proteome Res.* **10**, 4692-4702 (2011)

Abstract

Conserved from flies to human, the Hedgehog (HH) signaling pathway plays an important role in many developmental processes. But aberrant activation in adults has been linked to many types of cancer.

Recent data from our laboratory demonstrated that activation of Hedgehog signaling in mature murine white adipocytes leads to a reprogramming of the adipocyte, characterized by an increased glucose consumption and glycolysis, a shift to lactate production with a simultaneously decrease of mitochondrial function.

The goal of this diploma thesis was to study the effects of HH signaling on mitochondria of mouse adipocytes for the first time in more detail. To gain more insight we established a catalogue of mitochondrial proteomes of HH stimulated white adipocytes. Besides that we applied several techniques to characterize HH activated white adipocyte mitochondria. We used two mitochondria-specific dyes, namely Mitotracker Green FM and TMRE, to determine putative changes in mitochondrial distribution, biogenesis and membrane potential by FACS analysis and confocal microscopy. Quantitative PCR was performed to measure genes known to be involved in mitochondrial dynamics, i.e. mitochondrial fusion and fission as well as mitochondrial/genomic DNA ratios. Finally, electron microscopy was used to check for ultra-structural changes of Hedgehog stimulated mitochondria.

In summary, we could not observe any significant differences between HH activated white adipocytes and control cells in any mitochondrial characteristics tested. Therefore, we conclude that the reprogramming of mature white adipocytes by Hedgehog activation does not affect mitochondrial features, at least not in the first 48 hours after exposure to the HH stimuli.

Zusammenfassung

Der Hedgehog Signaltransduktionsweg ist konserviert von der Fliege bis zum Menschen und spielt eine wichtige Rolle in vielen Entwicklungsprozessen. Anomale Aktivierung im Erwachsenen wurde mit vielen Krebsformen in Verbindung gebracht.
Unser Labor demonstrierte vor Kurzem, dass die Aktivierung von Hedgehog in weißen Adipozyten der Maus zur Reprogrammierung des Adipozytenstoffwechsels führt. Diese ist charakterisiert durch einen erhöhten Glukoseverbrauch und eine erhöhte Glykolyse, eine Verschiebung hin zu vermehrter Laktatproduktion begleitet von einer gleichzeitigen Abnahme der mitochondrialen Funktion.
Aufbauend auf diesen Daten waren wir daran interessiert, die Effekte der Aktivierung des Hedgehog Signaltransduktionsweges auf die Mitochondrien genauer zu bestimmen. Eines unserer Hauptziele war die Etablierung eines mitochondrialen proteomischen Ansatzes, der leistungsfähig genug ist, die mitochondrialen Proteome von Hedgehog stimulierten weißen Adipozyten mit Kontrollzellen zu vergleichen. Darüber hinaus wendeten wir unterschiedliche Methoden, um die Mitochondrien in Hedgehog aktivierten weißen Adipozyten zu charakterisieren. Die zwei Mitochondrien-spezifischen Fluoreszenzfarbstoffe Mitotracker Green FM und TMRE wurden eingesetzt, um potentielle Änderungen in der mitochondrialen Verteilung, Masse und Membranpotential durch FACS Analyse und Konfokalmikroskopie zu bestimmen. Quantitative PCR wurde verwendet, um wichtige Gene der mitochondrialen Fusions- und Fissionsdynamik zu messen. Darüber hinaus bestimmten wir das Verhältnis von mitochondrialer und genomischer DNA, einen indirekten Marker für die Menge vorhandener Mitochondrien. Die Ultrastruktur der Mitochondrien wurde mit Elektronenmikroskopie untersucht.
Zusammenfassend bleibt festzuhalten, dass keine signifikanten Unterschiede in einer der erwähnten mitochondrialen Eigenschaften zwischen Hedgehog aktivierten weißen Adipozyten und Kontrollzellen zu finden war. Daraus schließen wir, dass eine 48 Stunden anhaltende Aktivierung des Hedgehog Signalweges die von uns gemessenen mitochondrialen Funktionen in weißen Adipozyten der Maus nicht beeinflusst.

Curriculum Vitae

Name:	**Lukas FRANK**
Mobile phone:	+43699/17244618
E-mail:	lukas.frank@gmx.net
Address:	Lerchenfelderstrasse 21/22
	1070 Wien
Date of birth:	01/03/1982 (Vienna)
Nationality:	Austria

Work experience

01/ 2011 – 01/ 2012	Univ. Doz. DDr. Harald Esterbauer Department of Medical and Chemical Laboratory Diagnostics Lazarettgasse 14, 1090 Wien Diplome thesis: *„Hedgehog signalling – studies on its impact on mitochondrial function in 3T3-L1 adipocytes*"
08/ 2010 – 09/ 2010	Mag. Dr. Josef Penninger IMBA – Institute of molecular biotechnology Dr.Bohrgasse 3, 1030 Wien Topic: *„Effects of miRNA-223 knock out in mice on mitochondrial biogenesis"*
09/ 2009	Ao. Univ. Prof. Mag. Dr. Andrea Gsur Institut für Krebsforschung Borschkegasse 8a, 1090 Wien Topic: *„Genetic polymorphisms in base excision repair genes and risk of colorectcal cancer"*
08/ 2009	Ao. Univ.-Prof. Mag. Dr. Ernst Müllner MFPL - Department of Medical Biochemistry Dr.Bohrgasse 9, 1030 Wien Topic: **„***Cell Size Control in Vertebrates - Evidence for a size-sensing mechanism in animal cells*"
12/ 2007 - present	Dr.Frank & Dr.Binder Institute of Radiology Eisenbahngasse 3, 2100 Korneuburg
2003 – 2007	Various temporary jobs
10/ 2001 – 09/ 2002	Rotes Kreuz Wien Nottendorfergasse 21; 1030 Wien Zivildienst

Education

10/ 2004 – 03/ 2012	Molecular biology studies University of Vienna
10/ 2002 – 09/ 2004	Human medicine studies University of Vienna
05/ 2001	Matura
1992-2001	Realgymnasium BGRG VIII Albertgasse 18-22, 1080 Wien
1988-1992	Volksschule Notre Dame de Sion Burggasse 37, 1070 Wien

Computer skills

Excellent skills in MS Office (Word, Excel, Powerpoint, Outlook)

Basic skills in GraphPad Prism, Scaffold, ImageJ, Adobe Photoshop

Scientific skills and lab techniques

Cell- and molecular biological methods
RNA/DNA isolation, PCRs, quantitative real-time PCR

Protein biochemical methods
Proteinisolation and isolation of subcellular fractions,
Western blotting, ELISA

Bioanalytic methods
1D-GeLC/MSMS

Cell culture
Cultivation- and harvest of common cell lines

Cell analysis
Flow cytometry

Cellular bioenergetic methods
XF extracellular flux analyzer (Seahorse Bioscience)

Microscopy
Confocal microscopy (LSM 700 – Carl Zeiss)

Language

German – native

English – fluent

French – basics

Interests

Since 1990	Teamsport fieldhockey (Austrian U21 national team) Traveling